Tuning features of assembly of polymer grafted particles by exploiting particle shape and polymer flexibility

By

Brandon Lin

A thesis submitted to the Faculty of the Chemical and Biological Engineering Department of the University of Colorado at Boulder in partial fulfillment of the requirement for the degree of the Master of Science

2014

Signature Page

This thesis entitled:

Tuning features of assembly of polymer grafted particles by exploiting particle shape and polymer flexibility

Written by: Brandon Lin

Has been approved by the department of Chemical and Biological Engineering

_____

Arthi Jayaraman – Chair

_____

Charles Musgrave

_____

Yifu Ding

Date: _____

The final copy of this thesis has been examined by the signatories, and we find that both the content and the form meet acceptable presentation standards of scholarly work in the above mentioned disciplines.

Abstract

Brandon Lin (M.S. Chemical Engineering)

Tuning Features of Assembly of Polymer Grafted Particles by Exploiting Particle Shape and Polymer Flexibility

Thesis Advised by Professor Arthi Jayaraman

We present a two-part computational study that demonstrates and explores new design parameters for the directed assembly of polymer grafted nanoparticles.

In the first part we present a predictive computational materials design study linking molecular features of the polymers to the structure and shape of the assembly of polymer functionalized nanoprisms. Focusing on nanoprisms with polymers grafted on their edges, we systematically vary monomer and solvent chemistry ranging from homopolymers in theta solvent and bad solvent, to AB copolymers with varying A and B solvent selectivity, and ratio of polymer molecular weight to particle size. In the absence of polymer functionalization the nanoprisms aggregate, when grafted with homopolymers in theta solvent the nanoprisms disperse, and when grafted with homopolymers in a bad solvent they assemble into one-dimensional stacks. When grafted with AB diblock copolymers in an A-selective solvent the nanoprisms form shell-like assembled structures. We find signatures of these many-body assemblies in a two-body potential of mean force (PMF) calculated using biased molecular dynamics simulations. For polymer grafted nanoprisms that assemble into stacks we find strong attraction at contact in the PMF, and for polymer grafted nanoprisms that assemble into shells we find strong attraction in the PMF at

appropriate inter-particle distances and orientations. As the functionalized polymer chain length to prism size decreases, the tendency to form shells decreases.

We present a molecular dynamics simulation study of systems containing homopolymer grafted particles in a homopolymer matrix, where the graft and matrix polymer chemistries are identical, to elucidate the effect of flexibility of the polymers on the wetting of the grafted layer by the matrix polymer and morphology of the nanocomposite. We find that decreasing flexibility of the grafted and matrix polymers causes the wetting of the grafted layer by the matrix polymers to increase. We also find that this increased wetting is more significantly driven by the graft flexibility than by the matrix flexibility. Due to this improved wetting of the grafted layer, we also observe increased particle dispersion in the polymer matrix.

Acknowledgements

This work acknowledges financial support by Department of Energy under Grant DE-SC0003912. This work also acknowledges the use of Janus supercomputer, which is supported by the National Science Foundation (award number CNS-0821794) and the University of Colorado Boulder. The Janus supercomputer is a joint effort of the University of Colorado Boulder, the University of Colorado Denver and the National Center for Atmospheric Research. I would like to thank Professor Arthi Jayaraman for her help, advice, and mentorship. I would also like to thank the members of our research group, specifically Tyler Martin, whose ideas and assistance contributed to the work presented here.

Table of Contents

Contents

List of Tables

List of Figures

I: Introduction

Growing emphasis is being placed on using computational methods to guide design of nanomaterials, specifically to tailor ligand functionalized nanoparticles to achieve a desired nanoparticle assembly and in turn, attain target macroscopic properties in optical, photonic, and photovoltaic applications.[1-3] The two aspects of functionalized nanoparticles, the nanoparticle itself and the grafted group can both affect the resulting assembly.

Much of the past computational work has focused on *spherical* particles functionalized with a variety of ligands including small molecule surfactants, synthetic macromolecules[4], biopolymers,[5-7] and polymers.[8-10] Recent advances in the field of nanomaterial synthesis has led to creation of particles with exotic and new non-spherical shapes, e.g. nanoprisms.[11-13] Motivated by these advances in nanomaterial synthesis, to accelerate materials discovery, computational scientists seek to provide the materials community with design rules on how to engineer nanomaterials that will direct these novel particle shapes into nanoclusters with unique structures not seen with spherical particles, and thus enable new applications that rely on assembled particles.[14] In this regard, we note extensive studies by Glotzer and coworkers who have used molecular simulations to predict assembly of oligomer functionalized nanocubes[15], nanorods[16], nanotriangles etc into various crystalline phases.[17-18] Similarly, using DNA ligands, Schatz and coworkers have simulated assembly of triangular particles, and shown that 1-D ordered assembly disappears when the DNA length is commensurate or less than the prism length.[19]

From the grafted perspective, a significant number of experimental and computational studies have elucidated the various design parameters that govern dispersion/assembly in polymer nanocomposites containing polymer functionalized nanoparticles.[20-27] Much of this past

work has been focused on particles functionalized with flexible and chemically identical graft and matrix chains. In this realm of chemically identical graft and matrix systems, the key parameters that have been shown to determine aggregation or dispersion of the grafted particles are polymer grafting density[22, 28], particle curvature,[29] molecular weights and polydispersity of the graft and matrix polymers.[30-34] At high grafting density, aggregation or dispersion of grafted particles is driven largely by dewetting or wetting of the grafted layer by matrix polymers. It is now well established that at high grafting density and on curved surfaces (e.g. nanospheres), when the molecular weight of the matrix polymer is less than the molecular weight of the graft, the grafted layer is wet by the matrix. This wetting of the grafted layer by the matrix results in increased mixing of polymer grafted particles and matrix chains and therefore increased particle dispersion. At low grafting density, larger molecular weight of graft chains shield the particle surface from interparticle attractive interactions, and promote particle dispersion.[35] Increasing particle size or decreasing surface curvature decreases the wetting behavior due to increased polymer crowding near the surface of the particle. Polydispersity in the molecular weight of the grafted polymers has been shown to eliminate the mid-range attractive well in the potential of mean force between polymer grafted particles and to stabilize particle dispersion.[30-34] In all of the above studies, the impact of polymer flexibility on wetting/dewetting and dispersion/aggregation has largely been left unexplored.

Several theoretical and simulation studies in the past have focused on systems of semi-flexible polymers (in the absence of nanoparticles)[36-51], near surfaces and interfaces,[51-56] as well as composites of semi-flexible polymers and bare particles.[57-60] For example, theory and simulations have shown semi-flexibility effects on coil to globule transition of the polymer chain,[39, 61] formation of spherical or toroidal globules as a function of semi-flexibility,[39, 47] and

isotropic-nematic liquid crystalline transitions. [37, 40, 41, 50] In a composite of semi-flexible polymers and bare nanoparticles near substrates, decreasing polymer flexibility causes an increase in polymer density near the surface, resulting in lower nanoparticle density near the substrate compared to flexible polymers.[58] Polymer semi-flexibility also impacts the depletion attraction in systems of particles and polymers, with the relative ratio of correlation length and persistence length dictating the depletion thickness and effects of particle curvature on depletion attraction[57]. All of these studies point to the importance of changing polymer flexibility on the polymer conformations as well as effective interactions between the bare particle/surfaces and polymers.

In Chapter 1, we present a molecular dynamics simulation study to create a design library linking molecular features of the polymer functionalized nanoprisms, such as the polymer chemistry and sequence (homopolymer versus copolymer), polymer molecular weight and particle size, solvent chemistry to the resulting nanoprism assembly. Figure 2 summarizes the qualitative behavior of the particle assembly as a function of the grafted polymer design. Additionally, we calculate potentials of mean force between polymer functionalized particles to capture the effective two-body effective interactions as a function of the polymer functionalization, and show that the signature of assembly of nanoprisms exists in the two-body effective interaction.

In Chapter 2, we present a second molecular dynamics simulation study to investigate a system of homopolymer functionalized spherical particles in a chemically identical homopolymer matrix to elucidate the effect of decreasing flexibility in polymer grafts and matrix on wetting of the grafted layer and nanocomposite morphology. We find that decreasing graft and matrix flexibility leads to increased wetting of the polymer grafted particles by the matrix

chains, and as a result improves the dispersion of particles with semi-flexible grafts. We show that changing the flexibility of the graft polymers has a more significant effect on improving wetting of the grafted layer than changing the flexibility of the matrix polymers do. We also quantify the effect of decreasing flexibility on the known trends of varying graft and matrix length and grafting density on wetting of the grafted layer by the matrix.

II: Effect of Particle Shape

Methods

Model Details

We simulate the assembly of coarse-grained (CG) polymer functionalized/grafted nanoprisms in an implicit solvent using molecular dynamics (MD) simulations in a canonical ensemble using graphical processing unit based HOOMD-blue package[62-64]. All CG beads in the particle and polymer have a diameter of 1nm. We model bare triangular nanoparticles as a rigid collection of hard spherical beads of unit diameter σ and mass. Each bead is placed recursively in a triangular pattern, with the length of the triangular nanoprism controlled by the number of rows of beads and width/height equal to bead diameter. For example, for a particle size (side length) of 5, there are 5 rows of beads that use a total of 15 beads; for a particle size of 7, there are 7 rows totaling 28 beads, and for a particle size of 11, there are 11 beads totaling 66 beads. We model the 6 polymer chains as permanently attached to the edge of the particle. One chain is attached to each of the vertices, and one chain is attached to the midpoint of each edge. For this reason, we are limited to only odd nanoprism lengths. Each grafted polymer strand is modeled as a bead-spring chain,[65] with each bead of size 1*nm* representing approximately a Kuhn segment of the polymer, and the springs linking them having a force constant of k=150 k_BT/nm^2 and a bond rest length of r_0=0.95nm.

$$U_{bond}(r) = \frac{1}{2} k_{bond}(r - r_0)^2 \quad (1)$$

where k is the force constant, r is the center to center distance between the bonded beads, and r_0 is the bond rest length.

The grafted polymers are either a homopolymer or symmetric AB diblock copolymer of 12 or 24 Kuhn segments or "monomers". In the case of the homopolymer, the monomer beads are denoted "M" and in the case of the copolymer, the beads of the inner block are denoted "A", and the beads of the outer block are denoted "B". Particle beads are denoted "P".

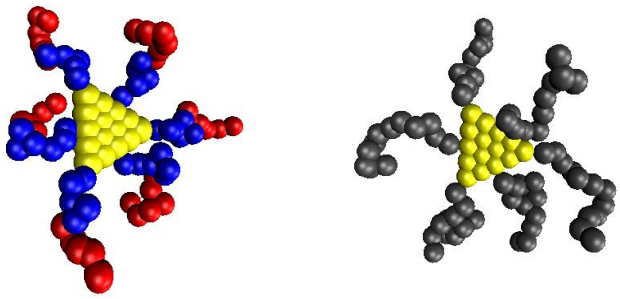

Figure 1: *Image of single copolymer grafted nanoprism (left) and single homopolymer grafted nanoprism (right)*

The chemical features of the model are tuned using either Lennard Jones(LJ)[66] potential or Weeks Chandler Andersen (WCA)[67] potential. The two faces of the nanoprism are considered to be either bare surfaces modeled using attractive particle-particle interactions or coated surfaces so as to shield particle-particle attractions. For the attractive case, LJ interactions between the CG beads of the nanoprism with cutoff distance r_{cutoff}=3.0, well depth ε=1,and rest distance σ=1 are used.

$$\begin{cases} U_{LJ}(r) = 4\varepsilon\left[\left(\frac{\sigma}{r}\right)^{12} - \left(\frac{\sigma}{r}\right)^{6}\right] & r < r_{cut} \\ U_{LJ}(r) = 0 & r > r_{cut} \end{cases} \quad (2)$$

where ε is the well-depth, σ is the rest distance, and r is the center to center distance. For the shielded case, athermal WCA interactions between the CG beads of the nanoprism with cutoff distance $r_{cutoff}= \sigma*2^{1/6}$, well depth ε=1,and rest distance σ=1 are used.

$$\begin{cases} U_{WCA}(r) = 4\varepsilon\left[\left(\frac{\sigma}{r}\right)^{12} - \left(\frac{\sigma}{r}\right)^{6}\right] + \varepsilon & r < r_{cut} \\ U_{WCA}(r) = 0 & r > r_{cut} \end{cases} \quad (3)$$

where ε is the well-depth, σ is the rest distance, and r is the center to center distance. Depending on the type of the polymer, the pair-wise monomer-monomer interactions are modeled using attractive LJ or athermal WCA potential as well. The well depth of the attractive LJ potential between two beads, i and j are denoted as ε_{ij} (units of k_BT) throughout the paper.

The well-depth ε of the former is used to describe the attractive strength between non-bonded monomers that are attracted to each other beyond their excluded volume and below the cut-off distance r_{cutoff}=3.0. Between each pair of beads where attractions were needed, attractive forces were modeled using and ε=0.5 or ε=1 depending on the system and σ=1 for all systems (Equation 2 above). For non-bonded monomers that face purely excluded volume interactions, we model those using WCA interaction with ε=1, σ=1 and $r_{cutoff}=\sigma*2^{1/6}$ (Equation 3 above). For all systems, a total of 30 polymer grafted particles is simulated.

Simulation Details

Simulations are run using HOOMD-blue[62-64] with the NVT Brownian dynamics integrator for both the rigid (particle beads) and nonrigid (polymer beads) groups in the system. Individual polymer grafted particles are grown with completely linear chains angled normal to the corresponding grafting point on the particle. Then, each particle is randomly placed within the simulation box while ensuring no overlaps. Systems are compressed at a temperature of 2 to 3.5 over 1 million timesteps from the initial configuration to a box size of 44 for the D=5, L=12 simulations. The first simulations were started at the higher temperature. After it became clear that the configurations of the system were just as disordered at lower temperatures, the initial

high temperature mixing step was run at lower temperatures. The volume fraction of beads in the box is kept constant across simulations at 0.0165. The simulation is then run at the same high compression temperature for 50 million timesteps before dropping in temperature in increments of 0.5 temperature units to the final temperature of 1.0 temperature units. Simulations continue until the final temperature is 1.0 temperature units and the system is equilibrated at that temperature. Multiple independent simulations were run for each interaction set, particle size, and strand length.

Analysis

Each of the major analysis metrics used, total coordination number, particle coordination number and domain numbers, are calculated in similar ways. The resulting simulation snapshot is organized into neighbor lists according to the metric being used. For the total coordination number, Z_{total}, a neighbor is defined as any member of one particle interacting with any member of another particle. For the particle coordination number, $Z_{particle}$, a neighbor is defined as any part of one particle interacting with any part of another particle (excluding the polymer grafts). Finally, for the number of domains, neighbors are defined as any A, B, or M monomer interacting with other monomer of the same type. In these cases, interacting is defined as a center to center distance of less than 1.25 distance units (bead diameter = 1), which was chosen to differentiate between clusters and maintain the level of connectivity seen visually. Coordination numbers are then calculated by averaging the number of neighbors of each particle. The number of domains is calculated by finding the number of clusters of each monomer according to the neighbor list.

One of the features of the particle coordination number is that shells intrinsically have lower coordination numbers than that of the stacks. Since the particles along the exterior of the shell do not actually interact, they ideal particle coordination number for that assembly is 0. By comparison, for stacks, the maximum particle coordination number would be 2, one particle on both the top and bottom surface of the particle. In the actual simulations, the finite size of the stacks results in the top and bottom particles on the stacks only having one neighbor; this reduces the particle coordination number from the ideal value.

The autocorrelation time was calculated for all systems. In order to have independent snapshots, data is only taken twice at the end of each simulation. One state is taken at the very end, and one state is taken 12.5 million steps previously. Error bars are then calculated by taking the standard error of both states for each of the five trials.

Potential of Mean Force Details

PMF calculations were performed using the WHAM (Weighted Histogram Analysis Method) software provided by the Grossfield lab.[68] In order to calculate the free energy landscape from the results of umbrella sampling simulations, the system was biased in two dimensions. Two grafted, triangular nanoparticles with various interaction sets were simulated and biased along the center to center distance of the particle and an angle metric describing the angle between the planes of the particles. The free energy profile is generated by WHAM for each separate angle along the interparticle distance coordinate.

In order to properly use the WHAM method, it is necessary to achieve overlapping windows over the measured quantities using harmonic potentials to bias the simulation. In order to sample

some of the possible angles between the particles in the system, a set of three three-body harmonic potentials were used to bias the angle between the particles. Each three-body potential connects one vertex of one triangle to its normal and to the corresponding vertex on the other triangle. With this method, an angle bias of 0° allowed the particles to preferentially sample the stacked configuration, while an angle bias of 90° allowed the particles to preferentially sample the edge-on configuration. In addition, angle biases of 30° and 60° were used. The free energy landscape was shifted to be zero for all angles at the furthest distance measured ($r_{center\text{-}to\text{-}center}$=20) to measure the free energy of assembly of the 2-particle system. The harmonic bond potential spring constant for the distance biasing, k was varied from 5-30 to insure there were no bond strength effects on the resulting free energy landscape. In addition, the spring constant for the angle biasing was varied from 250-500 for the same reason. The angle constant was necessarily much higher than the distance constant to restrict the particles to narrower windows.

$$U_{angle}(r) = \frac{1}{2}K(\theta - \theta_0)^2 \quad (4)$$

A window size of 0.5 distance units was used for the umbrella sampling, meaning that each bin center was 0.5 units apart. Data was output from the simulation every 1000 timesteps to insure independent snapshots, and only the last half of the dataset was used for calculation by WHAM. A tolerance of 10^{-4} was used in the WHAM software, and a temperature of 1 was specified. Due to the dimensionless units used, the Boltzmann's constant was defined as 1. Multiple trials for each free energy landscape were calculated for each system studied. In order to create the distance and angle histograms used to compare to the PMF results, data was taken from simulations run under the same conditions with 30 particles. Distance histograms were created by plotting the distribution of the nearest neighbor distances. Angle histograms were calculated using the angle biasing metric described previously and applied over each nearest neighbor pair

found for the distance histogram. A cutoff distance of 2 was chosen for the histograms to separate between stack distances and shell distances, in order to average the angles separately.

Results and Discussion

Figure 2 summarizes the qualitative behavior of assembly as the grafted polymer design and particle-particle attractions are varied.

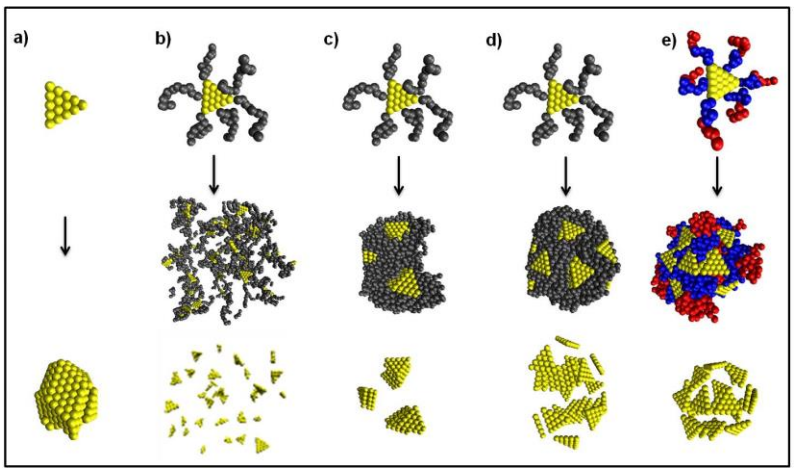

F*igure 2:* *Simulation snapshots of a) bare and (b-e) homopolymer or copolymer functionalized nanoprism, and their assembled or dispersed state. The five cases shown are: a) bare nanoprisms with attractive particle-particle interactions forming aggregates, b) athermal homopolymer grafted nanoprisms with attractive particle-particle interactions forming a dispersed state, c) attractive homopolymer grafted nanoprisms with attractive particle-particle interactions assembling into a stacked state, d) athermal homopolymer grafted nanoprisms with athermal particle-particle interactions assembling into a shell surrounded by stacks, and e) attractive copolymer grafted nanoprisms with athermal particle-particle interactions assembling into shells.*

Effect of grafting homopolymers on particle assembly/dispersion: A system of attractive (bare) nanoprisms with no polymer ligands assembles into aggregates with face-face stacking in multiple directions (Figure 2a). Grafting athermal homopolymers, i.e. homopolymers in a chemically similar solvent, to these attractive nanoprisms creates steric repulsions between the nanoprisms, resulting in completely dispersed particles (Figure 2b). Grafting attractive homopolymers, i.e. homopolymers in a chemically dissimilar or bad solvent, to these attractive nanoprisms causes the nanoprisms to align face-on into stacks, and the grafted (attractive) homopolymers guide the stacks to grow unidirectionally (Figure 2c). Turning off the particle-particle attractions, which one could achieve experimentally by coating the particle faces with surfactants, decreases the ability of the system to form clean stacks. Instead some nanoprisms

form stacks and others surround the stack to form a shell through attractive homopolymer interactions; we term these "shell surrounding stack" configurations (see appendix figure A.1).

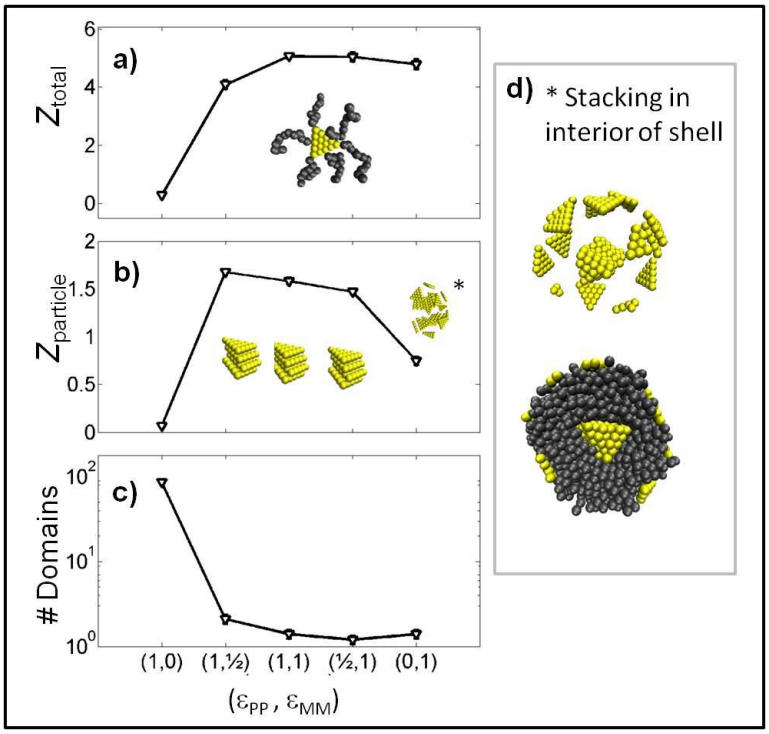

Figure 3: *Characterization of assembly/dispersion of homopolymer grafted nanoprisms as a function of particle-particle and monomer-monomer interaction strength (ε_{PP}, ε_{MM}) in units of k_BT. Average coordination number calculated based on a) monomer contacts, Z_{total} and b) particle contacts $Z_{particle}$, and number of polymer domains as a function of interaction strength. D) Simulation snapshot showing the "stacking in the interior of the shell" assembled state seen for (ε_{PP}, ε_{MM}) = (0,1) marked with an "*" in part b.*

Figure 3 shows quantitatively, as the monomer- monomer attraction within the polymer increases, which one could achieve experimentally by decreasing the solvent quality to homopolymer, at a constant particle-particle attraction strength of 1kT (the first three data points in the x-axis of Figure 3) the system goes from a dispersed state, marked by 0 coordination number (Figure 3a and 3b) and large number of domains (Figure 3c), to an aggregate with stacked particle arrangement, marked by a particle coordination number that is greater than 1 (Figure 3b) and few domains (Figure 3c). The increasing coordination numbers and decreasing

domain number is due to the increased ability of the monomers along the homopolymer strands to aggregate and form energetically favorable contacts. The particles transition from a dispersed state into a stacked aggregate as the monomer-monomer attraction is increased from a well depth ε_{MM} of 0 to 0.5kT. Any further increase in the attraction strength does not affect the stacking. As the particle-particle attraction is decreased or particle is shielded through surfactant coating at a constant polymer-polymer attraction strength of 1kT (the last three data points in the x-axis of Figure 3) the Z total and Z particle decrease while the number of domains remains low. Additionally as the particle-particle attraction decreases the particles no longer form clean stacks and instead form a combination of shells and stacks, specifically the "shell surrounding stack" configuration (Figure 3d).

Effect of grafting diblock copolymers on directing particle assembly: By grafting symmetric AB diblock copolymers, instead of homopolymers, one can drive the particles to align along their edges and form a spherical shell-like structure, where the exterior of the shell is the particles followed by a shell of the inner A monomers followed by a core of the outer B monomers (see supplementary figure A.2.). Such shell-like assembly is not observed in spherical nanoparticles, and is thus unique to nanoprisms. Figure 4 shows that these shell-like assemblies are obtained when nanoprisms are grafted on the edges with AB copolymers with χ~1, and in solvent that is either not selective to A or B or weakly selective towards B and on the faces coated with surfactants to shield particle-particle attraction. As the solvent selectivity towards B block is increased such that AA attraction strength is greater than BB attraction strength, the nanoprisms assemble into stacks rather than shells. The particle coordination number shows that the shells intrinsically have lower coordination numbers than that of the stacks. The reasons for

these trends are as follows. At ε_{BB}=0kT and 0.5kT, the enthalpic contribution from contacts between the (inner block) A monomer (ε_{AA} =1kT) dominates, which is maximized in the stack formation rather than shell formation. As the BB attraction strength increases to be commensurate with AA attraction, the particles adjust to the shell conformation (with some dimer stacks on the outside of the shell) as that is able to maximize the enthalpically favorable A-A and B-B contacts. At constant BB attraction strength of 1kT, as ε_{AA} reaches 0kT, which can be achieved with an A-selective solvent, the particles do not have a strong enough energetic drive to assembly and the nanoprisms are unable to form a shell, and aggregate into a poorly ordered state (denoted by a * in Figure 4b, and shown in supplementary figure A.3)

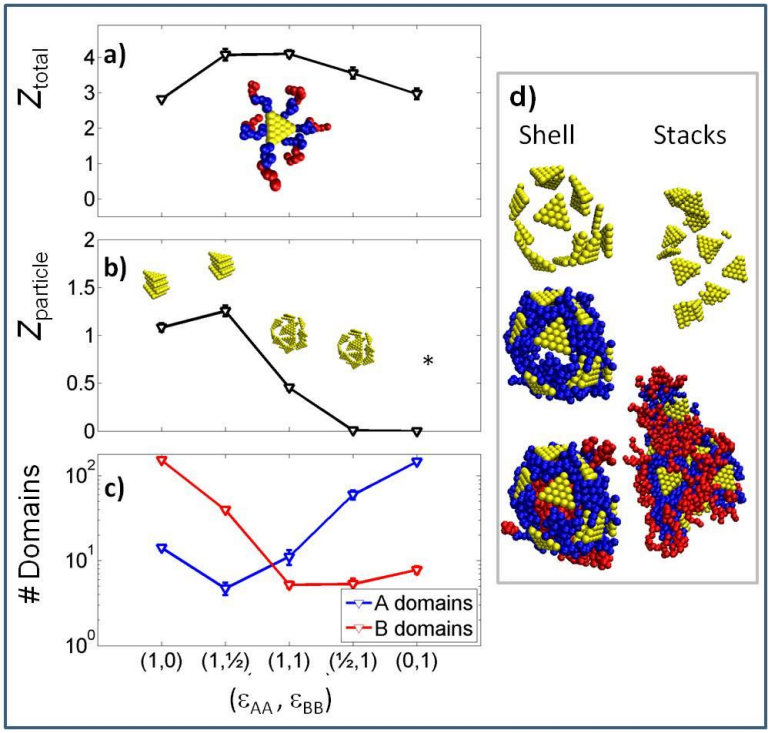

Figure 4: *Characterization of assembly/dispersion of diblock copolymer grafted nanoprisms as a function of monomer-monomer interaction strength (ε_{AA}, ε_{BB}) in units of k_BT. Average coordination number calculated based on a) monomer contacts, Z_{total} and b) particle contacts $Z_{particle}$, and number of polymer domains as a function of interaction strength. d) Simulation snapshots showing shells and stacks that form upon assembly for specific interactions.*

To understand if then tendency for shell-like assembly or stacked assembly or dispersed state has a signature in a two-particle effective interaction, we calculate the potential of mean force (PMF) between polymer grafted nanoprisms. Figure 5 presents the PMF for the three cases that showed the most different assemblies – dispersed state, stacks, shells, and shells with some partial stacking on the surface of the shells. The four angles shown in the Figure 5 capture the four orientations of two particles approaching each other, with 0° representing two particles parallel and stacked on top of one another, 90° representing two particles parallel to each other placed side by side, and 30° and 60° representing intermediate states. While the particles in reality would sample an ensemble of states, these 4 angles were chosen as they best distinguish the possible angles the particles sample in the various assemblies observed so far (see appendix figure A.4).

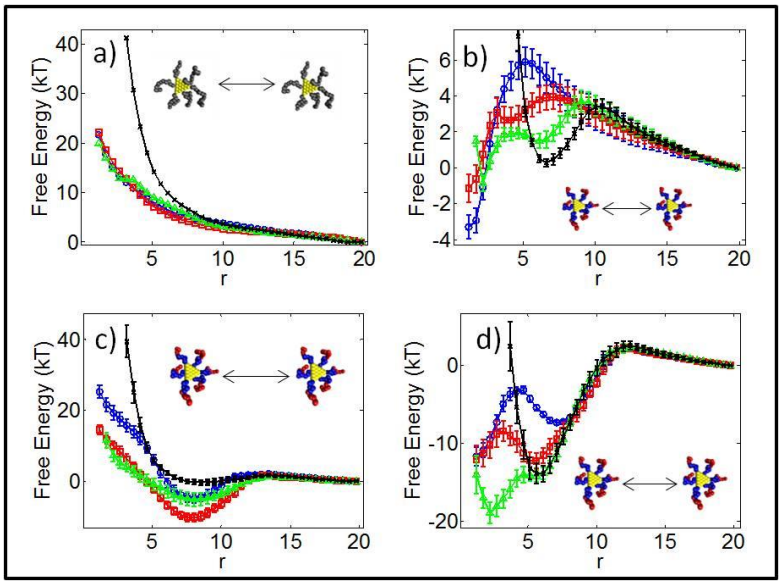

Figure 5*: Potentials of mean force (kT) between two grafted nanoprisms at 0° (blue circles), 30° (red squares), 60° (green triangles), and 90° (black crosses), for a) athermal homopolymer grafted on attractive nanoprisms that lead to dispersed state, b) diblock copolymer grafted athermal nanoprisms with (εAA, εBB) = (1,0) that assemble into stacks, c) diblock copolymer grafted athermal nanoprisms with (εAA, εBB) = (0,1) that assemble into poorly formed shells with no stacks, and d)) diblock copolymer grafted athermal nanoprisms with (εAA, εBB) = (1,1) that assemble into shells with small stacks on the surface of the shells.*

Figure 5a captures the steric repulsion in the case athermal homopolymers grafted on attractive nanoprisms, which drives the dispersion of the nanoprisms. When diblock copolymer grafted nanoprisms assemble into a stacked state the average inter-particle distance is 1.57 +/- 0.16 (appendix figure A5 left column) and average orientation (as defined in the methods section) is 25.5 +/- 3.6 (supplementary figure S.5 left column). The 0° and 30° PMFs in Figure 5b show strongest (4kT) attraction at inter-particle distance <2.5nm. All other curves and inter-particle distances show less favorable PMF. When diblock copolymer grafted nanoprisms assemble into poorly-ordered aggregate (with no stacks) state the average inter-particle distance is 6.90 +/- 0.27 (supplementary figure S.5 middle column) and average orientation is 50.9 +/- 3.5 (supplementary figure S.5 middle column). Figure 5c shows that the PMF is attractive only in the range of inter-

particle distances 5-10nm for 0° and 60°. When diblock copolymer grafted nanoprisms proceed to shell-like assembly with some dimer stacks on the outside of the shell, the average inter-particle distance is 3.42 +/- 0.17 (supplementary figure S.5 right column) and average orientation is 43.4 +/- 3.5 (supplementary figure S.5 right column). The PMF in Figure 5d shows most favorable free energy for 60° at inter-particle distances 0nm <r <5nm, for 30° at inter-particle distances 0nm <r <2nm and 5nm>r>8nm, and for 0° at inter-particle distances 0nm <r <2nm. As the states that are most favorable in the two-particle free energy or PMF are the same as the states sampled in the many particle assembly, this eludes to the fact that tendency of various assemblies have a signature in the effective interactions.

In summary, when particle-particle attraction is negligible, when AA attraction is dominant (i.e. B selective solvent) it favors stack formation, when BB attraction is dominant (i.e. A selective solvent) it favors shell formation, and when AA and BB attractions are commensurate (non-selective solvent) it favors shell formation with a few small stacks on the shell exterior. In general, there are more A domains than B domains because the A monomers on the inner block have to stretch much more than the B monomers to get to a neighboring A block. This chain grafting constraint on the A blocks causes B monomers to aggregate easily into fewer B domains than A monomers can into A domains. This can be reversed however in the cases where particle-particle attraction outweighs the monomer-monomer attractions. In these cases, there is greater drive for the A monomers to assemble by virtue of being closer to the particle surface that is also trying to make other particle surface contacts.

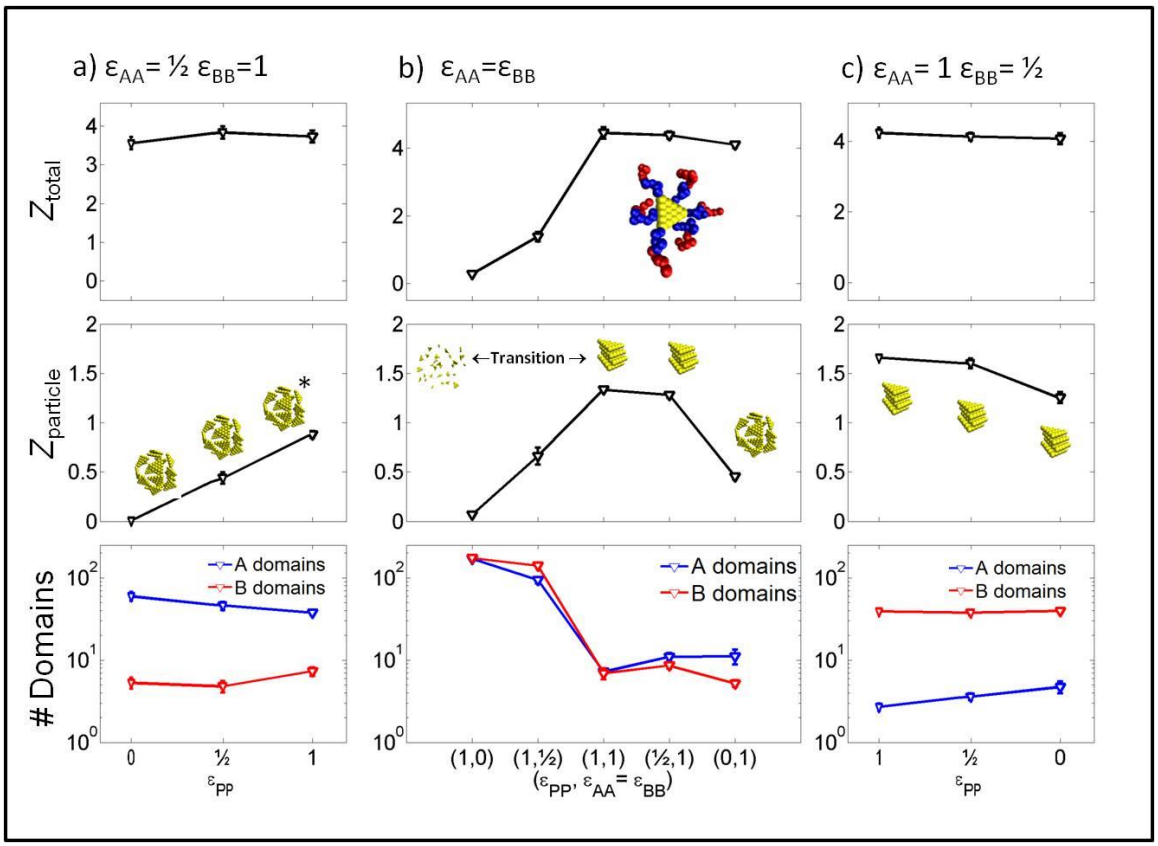

Figure 6: *Characterization of assembly/dispersion of copolymer grafted nanoprisms as a function of particle-particle and monomer-monomer interaction strength (ε_{PP}, ε_{AA}, ε_{BB}) in units of k_BT. Average coordination number calculated based on a) monomer contacts, Z_{total} and b) particle contacts $Z_{particle}$, and number of A and B domains as a function of interaction strength.*

To further understand the impact of competing particle-particle and monomer-monomer attractions on AB diblock copolymer grafted nanoprism assembly, we increase ε_{PP} to 1kT for three cases: when i) $\varepsilon_{AA} = \varepsilon_{BB,}$ ii) $\varepsilon_{AA} < \varepsilon_{BB,}$ and iii) $\varepsilon_{AA} > \varepsilon_{BB}$ (Figure 6).

At ε_{PP}=1kT and increasing monomer-monomer attraction, while maintaining $\varepsilon_{AA} = \varepsilon_{BB,}$ the particles transition from a dispersed state to stacked state for (Figure 6b) with the particle-particle attraction being the biggest driving force for the stacking. This is also evident from the fact that at $\varepsilon_{AA} = \varepsilon_{BB}$=1kT, and increasing ε_{PP} from 0kT to 1kT (Figure 6b) the particles go from

shell arrangement to stacked arrangement. We also note that the increase in the coordination numbers is much steeper when increasing particle attraction at constant polymer attraction ε_{AA} = ε_{BB} =1kT, than that seen when increasing polymer attraction at constant particle attraction ε_{PP} of 1kT. In the case where ε_{AA} =0.5 and ε_{BB} =1.0 (Figure 6a), increasing particle-particle attraction leads to increasing particle ⟨Z⟩ and slightly decreasing number of A domains. Since AA attraction is relatively low, adding particle-particle attraction causes the particles to get into stacked formation and as a result reduces the number of A domains. The total ⟨Z⟩ and number of B domains remain constant. The particle-particle attraction does not appreciably change the clustering of the B monomers or the overall clustering because the effect is more localized. In the case where ε_{AA} =1.0 and ε_{BB} =0.5 (Figure 6c), increasing particle-particle attraction strength leads to a less dramatic increase in particle ⟨Z⟩. Since the AA attraction is relatively high, increasing the PP attraction only has a small effect on the ability of the particles to stack; the particles stack to primarily maximize AA contacts. The number of B domains and total particle ⟨Z⟩ remain unchanged by increasing ε_{PP} for the same reason. However, the number of A domains decreases slightly with the increase in PP attraction due to particles coming closer in proximity and increasing A monomer aggregation.

Effect of polymer strand length on assembly of polymer grafted nanoprisms: In the case of homopolymer grafts in the absence of particle-particle attraction as the graft length is increased, while maintaining particle size constant, the coordination number decreases (appendix figure A.6), due to higher number of monomers in the longer grafts causing larger steric hindrance as the particle get close together due to larger number of grafted monomers. As a result of the increased steric repulsion, the particles are farther apart, and the number of polymer domains

increases with increasing graft length. The overall trends in coordination number and number of domains with varying particle-particle and monomer-monomer interactions is maintained for the higher homopolymer length. In terms of assembly shape the particle clusters shift from the stack configuration towards the shell configuration (see snapshots in appendix figure A.6).

In the case of copolymer grafts, in the absence of particle-particle attraction $\varepsilon_{PP}=0$ (appendix figure A.7), when $\varepsilon_{AA}\geq\varepsilon_{BB}$ as graft length increases the particle coordination number decreases, and number of B domain also decreases, while number of A domains remains constant. The effect of length on the cluster shape is reduced compared to the homopolymer case. There is still a shift towards more shell formation, but only at low BB attraction strength. This is because increasing graft length increases the number of A monomers, and since AA attraction is dominant, the particles aggregate to maintain A monomers aggregation. In this process the B monomers, which are also larger in number for the longer grafts, are able to get together more, due to a larger inner A block, leading to fewer B domains. Since the polymers are aggregating around the non-attractive particles, the particles are spaced farther apart, decreasing the particle coordination number. In contrast, when $\varepsilon_{BB} > \varepsilon_{AA}$, as graft length increases the particle coordination remains the same and almost equal to 0; this is due to the system with the longer polymers maintaining the shell formation seen for the shorter graft lengths. The number of A domains remain constant when $\varepsilon_{AA} =0$ and decreases when $\varepsilon_{AA} =1/2kT$. The number of B domains remains fairly constant with changing graft length.

In the case of copolymer grafts in the presence of particle-particle attractions (appendix figure A.8), the graft length has a much smaller effect on the particle assembly, specifically the

coordination numbers, as compared to the effect in the absence of particle-particle attraction (appendix figure A.7). The longer strand lengths have higher total coordination numbers (Z_{total}) due to the larger reach of each strand, and thus more particles counting as neighbors than shorter strand lengths.

Effect of particle size on assembly of diblock copolymer grafted particles: The effect of the particle size at constant polymer length is studied in the absence of particle-particle attraction, as we cannot fairly compare the various cases of particle sizes since increasing particle size also increases the net particle-particle attraction. Thus, in the absence of particle-particle attraction, when AA attractions are dominant $\varepsilon_{AA} > \varepsilon_{BB}$, as particle size increases (Figure 7), the number of A domains increases with size much more than number of B domains. Similarly, when $\varepsilon_{BB} > \varepsilon_{AA}$ as particle size increases, the number of B domains increases with size much more than number of A domains. However, the effect of particle size is more drastic on the number of A domains than on the number B domains. As the particle size increases, the copolymers are grafted farther apart in the particle, making it difficult for the grafts on the same particle to interact, and thus increasing the net number of domains. The impact of the farther grafting is more on the A monomers than B monomers, due to the closer proximity of A monomers to the particle surface, leading to the asymmetry in particle size effect.

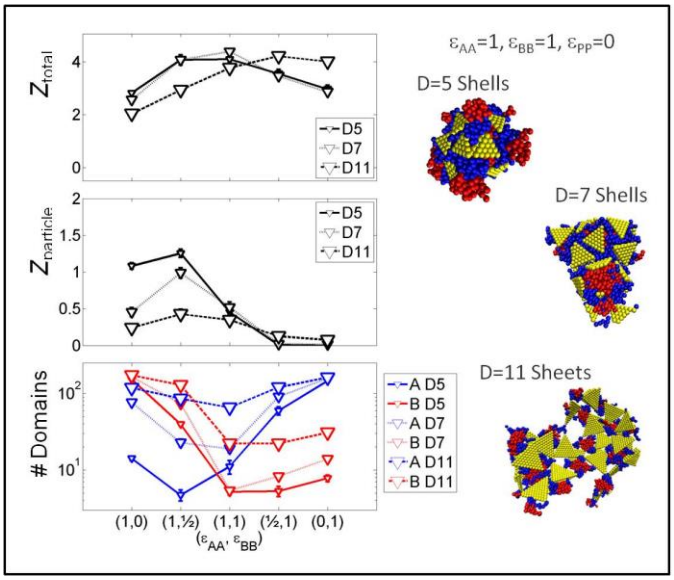

Figure 7: *Characterization of assembly/dispersion of copolymer grafted nanoprisms as a function of particle-particle and monomer-monomer interaction strength (ε_{PP}, ε_{AA}, ε_{BB}) in units of k_BT for increasing particle size (D=5, 7 and 11nm) at constant graft length of 12 monomers. Average coordination number calculated based on a) monomer contacts, Z_{total} and b) particle contacts $Z_{particle}$, and c) number of A and B domains as a function of interaction strength. Also shown are select simulation snapshots for one specific interaction set.*

In terms of assembly, nanoprisms of sizes 5 and 7 have similar total coordination numbers, as the number of monomers aggregating is not significantly different. As the particle size is further increased to 11 however, the total coordination number is lower than the smaller particle sizes when $\varepsilon_{AA} > \varepsilon_{BB}$ due to the A monomers' inability to make inter-graft contacts and connect particles. Increasing BB attractions increases the driving force for the particles of size 11 to form more inter-particle contacts increasing the total coordination number. Additionally, the total coordination number of particles of size 11 becomes higher than that of particles of size 5 and 7 when $\varepsilon_{BB} > \varepsilon_{AA}$ because the larger particles are unable to aggregate into shell-like assemblies seen at smaller particle sizes (see snapshots in the appendix figure A.9). Due to the much smaller strand length to particle size ratio, the larger particles have trouble forming inter-graft attractive monomer contacts that are needed to form the shell structure. Instead, the larger particles align

edge on to another particle to maximize their polymer contacts with one other particle, or edge on to an existing cluster of polymers to maximize their contacts that way. The first method tends to form sheets of particles (Figure 7 bottom right corner) while the latter forms more disordered aggregates with pieces of sheets (appendix figure A.9).

Therefore, as the particle size increases, at conditions where stack formation was observed for smaller particles, the propensity for stack formation decreases as characterized by the decrease in $Z_{particle}$. For chemistries where shell formation is seen in smaller particles, the propensity for shell formation decreases as the particle size increases. In order to maintain shell formation with larger particles, the average angle between particles should decrease significantly because fewer particles can fit in an individual shell cluster. Instead, the average angle does not change much, suggesting the larger particles prefer to maintain similar number of monomer contacts as the smaller particles and not form shell-like assemblies.

Conclusion

In summary, using molecular dynamics simulations we have shown how various design features of the polymer functionalization impact the assembly of the functionalized nanoprisms. Complex interplay of competing particle-particle interactions and monomer-monomer interactions and particle size to graft length ratio dictate whether the nanoprisms stay dispersed, aggregate into stacks or assemble into shell-like clusters. The propensity of nanoprisms to form these assembled structures is captured in the potentials of mean force The variety of assembled structures – stacks, shells, shell surrounding a stack- these particles sample demonstrate their applicability in engineering materials for metamaterials, delivery applications, etc.

III: Effect of Polymer Flexibility

Method:

Model

We model polymer grafted spherical nanoparticles in a polymer matrix using a generic coarse-grained model, where the nanoparticles are modeled as a rigid-body of several d=1σ beads (σ ≈ 1nm), and the polymers as bead-spring chains. The nanoparticle consists of surface beads to preserve the excluded volume of the particle and grafting sites to anchor the grafted chains. The surface and grafting site beads overlap in the rigid body of the particle, with the grafting site beads isotropically located in the spherical particle surface. Each grafted or matrix polymer is modeled as a bead-spring chain,[65] with each bead of size d=1σ representing a group of monomers on the polymer chain, and harmonic springs linking the beads having a force constant of k_{bond}=50 k_BT/σ^2 and a bond rest length of r_0=1σ, mathematically represented as

$$U_{bond}(r) = \frac{1}{2} k_{bond}(r - r_0)^2 \quad (5)$$

where *r* is the center to center distance between the bonded beads.

We model decreasing flexibility in the graft and matrix polymers through a harmonic angle potential with varying force constant of K=0-10 k_BT/radians^2, and a rest angle of $\theta_0=\pi$ radians, mathematically represented as[69]

$$U_{angle}(r) = \frac{1}{2} K_X(\theta - \theta_0)^2 \quad (6)$$

where X is graft or matrix, and θ is the angle between the two bond vectors that define the potential

We model a purely athermal system where all pairs of coarse-grained beads, including grafted, monomer, and surface beads, interact via the Weeks-Chandler-Andersen[67] (WCA) potential.

$$\begin{cases} U_{WCA}(r) = 4\varepsilon\left[\left(\frac{\sigma}{r}\right)^{12} - \left(\frac{\sigma}{r}\right)^{6}\right] + \varepsilon & r < r_{cut} \\ U_{WCA}(r) = 0 & r > r_{cut} \end{cases} \quad (7)$$

where ε=1 (in units of k_BT), σ=1 and $r_{cut}=\sigma*2^{1/6}$

In this study the nanoparticle size is maintained at 5σ, grafting density is varied from 0.25 to 0.65 chains/σ^2, the matrix polymer length is varied from 20-100 coarse-grained beads, the graft polymer length is varied from 10-40 beads, and the angle potential force constant is varied from 0 to 10 k_BT/radians^2, with the majority of the results shown for 0 and 5 k_BT/radians^2. The total occupied volume fraction in the simulation box is maintained to be 0.1 for all systems and the number of grafted particles is varied from 1 to 20 particles. For single particle simulations, we use 60,000 matrix beads and for multi particle simulations we use 120,000 matrix beads. The simulation box volume for single particle simulations is about 68x68x68 σ^3, and for multi particle simulations is about 91x91x91 σ^3.

Simulation Details

Using the model described above, we conduct Brownian dynamics (BD) simulations in the canonical ensemble using the graphical processing unit based HOOMD-blue package.[62-64] We first create an initial configuration in the following manner: We generate a particle of a desired diameter with isotropically distributed graft points, with the chains extending radially from these graft points embedded on the particle surface. In order to make it easier to insert the grafted particle into the simulation box, a short simulation with strong Lennard-Jones monomer-

monomer and monomer-particle attraction is then run to compress the grafted chains from these extended conformations. We note that this is the only time we use attractive non-bonded interactions in our simulation, as the study is focused on a system with athermal interactions. Copies of this one compressed grafted nanoparticle are then randomly placed in a large cubic box to achieve the desired number of particles along with the desired number of matrix chains. This initial configuration is then integrated using a Brownian dynamics integrator for 0.5e6 time steps to both mix and relax the grafted and matrix chains. The box is then compressed to the desired volume fraction over 0.5e6 steps, and then mixed again for 0.5e6 steps at the compressed state. Using this relaxed initial configuration at the appropriate packing fraction at reduced temperature T*=1, we finally conduct the production simulation runs for at least 40 million time steps where snapshots of the system are saved every 0.1e6 time steps.

Analysis

We calculate a number of structural features (e.g. monomer concentration profiles, radii of gyration, graft and matrix end-end distances) and thermodynamic information (e.g. mixing entropy. Data is calculated from 200 independent uncorrelated snapshots, with the error bars calculated as the standard error between these 200 data points.

We quantify monomer concentration profiles of the grafted and matrix chains from the particle surface as follows:

$$C_X(r) = \frac{\langle n_X(r) \rangle}{4\pi r^2 \Delta r} \quad (8)$$

where $C_x(r)$ (X=graft or matrix) is the monomer concentration profile, in units of $\sigma^{(-3)}$, as a function of r, the distance between the particle surface and the monomer, and $\langle n_X(r) \rangle$ is the average number of monomers of type X that are within a shell of thickness Δr at distance r.

The brush height defines the effective thickness of the grafted layer of the grafted particle and is calculated as the root mean square of the distance of the grafted beads from the surface of the particle.

$$\langle H_B^2 \rangle^{0.5} = \sqrt{\frac{1}{(n_P * n_G)} \sum_{i=1}^{n_G} r_i^2} \tag{9}$$

where $\langle H_B^2 \rangle^{0.5}$ is the brush height in units of σ, r_i is the distance of the i^{th} graft monomer from the surface of the particle the graft belongs to, n_P is the total number of grafted particles, and n_G is the total number of graft monomers in the system (across all grafted particles).

The average end-to-end distance of the polymer chain is calculated by averaging the distance between the first and last monomer of each matrix chain over the number of matrix chains in the system:

$$\langle R_{ee}^2 \rangle = \frac{1}{n_{MC}} \sum_{i=1}^{n_{MC}} \left(r_{i,n} - r_{i,1} \right)^2 \tag{10}$$

where $\langle R_{ee}^2 \rangle$ is the average squared end to end distance of the matrix chains, in units of σ^2, n_{MC} is the number of matrix chains, and $r_{i,n}$-$r_{i,1}$ is the distance between the first and last monomers of the i^{th} chain.

The average radius of gyration of the grafted chains quantifies the size of the grafted chain conformations averaged over all of the grafted chains in the system.

$$\langle R_g^2 \rangle = \left(\frac{1}{n_{GC} * N_G} \right) \sum_{i=1}^{n_{GC}} \sum_{j=1}^{N_G} \left(r_{i,j} - r_{i,com} \right)^2 \tag{11}$$

where $\langle R_g^2 \rangle$ is the average squared radius of gyration, in units of σ^2, n_{GC} is the number of grafted chains in the system(across all particles), N_G is the length of the grafted chains, $r_{i,j}$ is the position of monomer j on chain i, and $r_{i,com}$ is the center of mass of chain i.

The wet matrix bead percentage quantifies the degree of wetting of the grafted layer by matrix monomers:

$$\text{wet matrix } \% = \frac{n_{M,wet}}{n_M} (100\%) \quad (12)$$

where n_M is the total number of matrix monomers in the system and $n_{M,wet}$ is the number of matrix monomers that are within the brush height ($\langle H_B^2 \rangle^{0.5}$) i.e. the number of monomers that have wet the grafted layer of any particle.

We also calculate the particle-particle pair correlation function, $g_{PP}(r)$, which describes the extent of aggregation/dispersion of the grafted particles in the polymer matrix, by quantifying the correlation between the particle centers.[70] This is calculated only for the systems with multiple grafted particles.

We also estimate the total gain in mixing entropy upon the matrix chains wetting the grafted layer, $T\Delta S_{wet}$, as shown below in Equation 10. We calculate this quantity using

$$T\Delta S_{wet} = -\frac{k_B}{N_M} \sum_{n_{M,wet}=1}^{\langle n_{M,wet} \rangle} \ln \frac{\phi_{M,wet}}{\phi_{M,unwet}}$$
$$\phi_{M,wet} = \frac{n_{M,wet}}{n_{M,wet} + n_{G,wet}}, \qquad \phi_{M,unwet} = \frac{n_M - n_{M,wet}}{n_M + n_G - \left(n_{M,wet} + n_{G,wet}\right)} \quad (13)$$

where $T\Delta S_{wet}$ is the total gain in mixing entropy, in units of k_BT, k_B is Boltzmann's constant, N_M is the length of the matrix chains, $\phi_{M,wet}$ is the volume fraction of matrix monomers that have wet the grafted layer, and $\phi_{M,unwet}$ is the volume fraction of matrix monomers that are outside the grafted layer. Since the volumes of the individual matrix and grafted monomers are equal, the volume fractions can be calculated as number fractions, where n_M is the total number of matrix monomers in the system, $n_{M,wet}$ is the number of wet matrix monomers, n_G is the total number of graft monomers in the system, and $n_{G,wet}$ is the number of wet graft monomers. We calculate the

number fractions by explicitly counting graft and matrix monomers in the simulation that are within the brush height and averaging that value over snapshots and independent trials.

Results

Effect of polymer flexibility on wetting of the grafted polymer layer by matrix polymers

Figure 8 shows schematics and the ensemble average graft monomer concentration profile for a single homopolymer grafted nanoparticle in a chemically identical homopolymer matrix for completely flexible polymers and polymers with reduced flexibility. As the graft and matrix polymer flexibility decreases, marked by an increase in K (K_{graft} and K_{matrix}), the shape of the monomer concentration profile changes. With decreasing flexibility, the grafted chains adopt extended conformations, reaching farther distances from the particle surface, thereby increasing the brush height from the particle surface. With decreasing polymer flexibility, the concentration profile of matrix chains extends further into the grafted layer, implying increasing wetting of the grafted layer by the matrix chains.

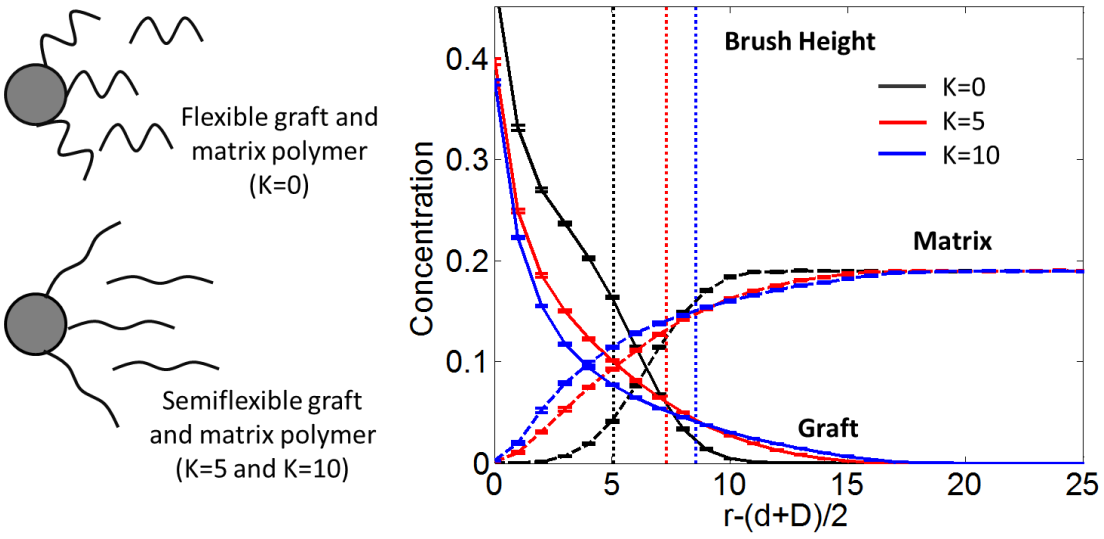

***Figure 8**: Schematic of polymer grafted nanoparticle and matrix polymer with varying flexibilities. Graft (solid) and matrix (dashed) monomer concentration profile for a single polymer grafted particle with particle diameter 5nm, polymer grafting density=0.65 chains/σ^2, graft length=20 segments, and matrix length =60 segments. Decreasing flexibility is denoted by*

increasing values of three-body angle constant $K=K_{graft}=K_{matrix}=0$ (black), 5(red) and 10 (blue) k_BT/radians^2. *The grafted layer brush heights, $\langle H_B^2 \rangle^{0.5}$, for varying flexibilities are shown as vertical dash-dotted lines.*

Since we maintain athermal interactions in these simulations, the wetting/dewetting of the grafted layer by matrix chains is driven by the balance of gain in mixing entropy and losses in conformational entropy of the grafted and matrix chains upon wetting. Decreasing flexibility of the *matrix* polymer is expected to decrease its conformational entropy in the bulk, and as a result decrease the conformational entropy loss the matrix chain would face upon entering/wetting the crowded grafted layer. As expected, as matrix flexibility decreases, the average end-end distance of the matrix polymer increases (see Table 1); the average and the distribution of end-end distances is a signature of the conformational entropy of the matrix chains. While decreasing *graft* polymer flexibility also reduces the conformational entropy loss of the grafted chains upon being wet, the conformational entropy loss of the grafted chains is relatively negligible when compared to the matrix due to the grafts being constrained to the particle surface and crowded by other grafts. More importantly, decreasing *graft* flexibility increases the brush height (denoted by dashed-dotted lines in Figure 8), which in turn increases the grafted layer volume and likely the mixing entropy gain upon wetting (discussed below in detail). Overall, by decreasing the flexibility of the grafted and matrix chains, the conformational entropy losses upon wetting of the grafted layer are reduced, while the gains in mixing entropy are increased, driving the increased wetting of the grafted layer, as seen in Figure 8. Next, to understand which of these two factors – reduction in conformation entropy loss upon wetting or gain in mixing entropy upon wetting – more significantly drives the increased wetting of the grafted layer by matrix chains with decreasing polymer flexibility, we tune the graft and matrix flexibility individually.

Table 1: End to End Distance

K_{graft}	K_{matrix}	Grafting Density (chains/σ^2)	N_{graft}	N_{matrix}	Graft $\langle R_{end\text{-}end}^2\rangle^{0.5}$ (units of σ)	Stdev Graft $\langle R_{end\text{-}end}^2\rangle^{0.5}$ (units of σ)	Matrix $\langle R_{end\text{-}end}^2\rangle^{0.5}$ (units of σ)	Stdev Matrix $\langle R_{end\text{-}end}^2\rangle^{0.5}$ (units of σ)	Wet Matrix $\langle R_{end\text{-}end}^2\rangle^{0.5}$ (units of σ)	Stdev Wet Matrix $\langle R_{end\text{-}end}^2\rangle^{0.5}$ (units of σ)	Unwet Matrix $\langle R_{end\text{-}end}^2\rangle^{0.5}$ (units of σ)	Stdev Unwet Matrix $\langle R_{end\text{-}end}^2\rangle^{0.5}$ (units of σ)
0	0	0.65	20	60	8.3	1.9	12.6	4.5	12.6	4.6	12.6	4.5
0	5	0.65	20	60	8.2	1.9	24.1	7.9	23.6	8.2	24.1	7.9
5	0	0.65	20	60	12.8	2.7	12.6	4.5	12.7	4.5	12.6	4.5
5	5	0.65	20	60	12.9	2.6	24.0	8.0	23.9	8.0	24.0	8.0
10	10	0.65	20	60	15.2	2.2	30.8	8.0	30.8	8.0	30.8	8.0
0	0	0.25	20	60	7.3	2.0	12.6	4.5	12.5	4.6	12.6	4.5
5	5	0.25	20	60	12.6	2.8	24.0	7.9	23.9	7.9	24.0	7.9
0	0	0.65	20	20	8.3	1.9	6.7	2.1	6.7	2.1	6.7	2.1
5	5	0.65	20	20	12.9	2.7	12.4	2.9	12.4	2.9	12.4	2.9
0	0	0.65	10	60	5.1	1.1	12.6	4.5	12.	5.2	12.6	4.5
5	5	0.65	10	60	7.4	1.0	24.0	7.9	23.9	7.8	24.0	7.9
0	0	0.65	40	60	12.6	3.2	12.6	4.5	12.6	4.5	12.6	4.5
5	5	0.65	40	60	20.4	5.6	24.0	8.0	23.9	8.0	24.1	8.0
0	0	0.65	20	40	8.2	1.9	10.0	3.5	10.2	3.4	10.0	3.5
5	5	0.65	20	40	12.9	2.7	19.2	6.0	19.3	6.0	19.2	6.0

Table 1*: Average end-end distance of the graft and matrix polymers for varying graft and matrix lengths, grafting densities, and flexibilities. The graft and matrix end-to-end distances is defined as the average over all of the graft and matrix chains respectively. The "wet matrix" end-to-end distance is defined as the average over any chain that has any bead within the grafted layer "brush" height, $\langle H_B^2\rangle^{0.5}$, and the "unwet matrix" end-to-end distance is the average over the remainder of the chains. The standard deviation of the independent snapshots is the error shown.*

Figure 9 shows the graft and matrix monomer concentration profiles as the graft and matrix flexibility are varied individually. The concentration of matrix beads at short distances from the particle surface within the brush height is higher and thus, the grafted layer wetting is larger, for decreased *graft flexibility* ($K_{graft}>0$, $K_{matrix}=0$) than for decreased *matrix flexibility* ($K_{graft}=0$, $K_{matrix}>0$). Similarly, the percentage of matrix beads that have wet the grafted layer, as shown in Table 2, is significantly more for the case of $K_{graft}>0$, $K_{matrix}=0$ than that for the $K_{graft}=0$, $K_{matrix}>0$ case, indicating that decreasing graft flexibility improves wetting more than decreasing matrix flexibility does. At constant graft flexibility, decreasing the flexibility of the matrix polymer has little effect on the brush height, and therefore little effect on the volume of the grafted layer. This suggests that when the graft polymer is flexible and matrix polymer flexibility is reduced, any changes in wetting have to come solely from the matrix chains losing

less conformational entropy upon wetting the grafted layer and not from increases in mixing entropy.

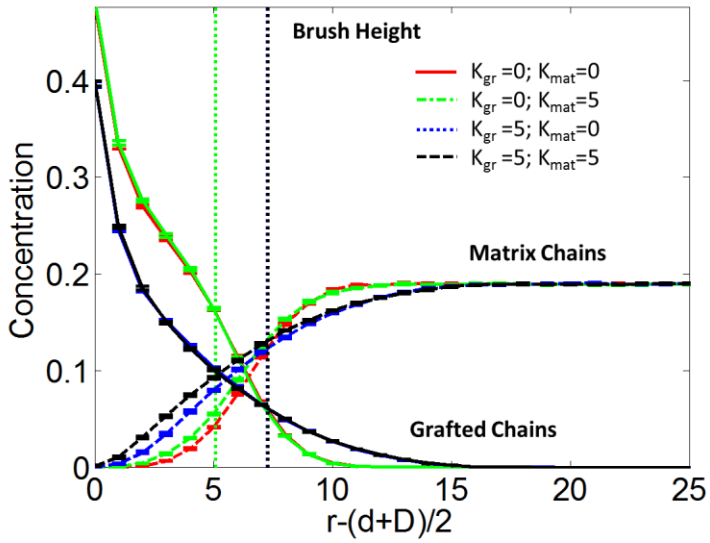

Figure 9*: Graft (solid) and matrix (dashed) monomer concentration profile for single polymer grafted particle with particle diameter 5nm, polymer grafting density=0.65chains/σ^2, and graft length=20 and matrix length =60 segments. The grafted layer brush heights , $\langle H_B^2 \rangle^{0.5}$, are shown with dotted lines. The four colored lines correspond to K_{graft} =0 and K_{matrix} =0 (red), K_{graft} =0 and K_{matrix} =5 (green), K_{graft} =5 and K_{matrix} =0 (blue), and K_{graft} =5 and K_{matrix} =5 (black).*

Table 2 Percentage of wet matrix monomers within grafted layer

K_{graft}	K_{matrix}	Grafting Density (chains/σ^2)	N_{graft}	N_{matrix}	Wet Matrix %	Error
0	0	0.65	20	60	0.03%	0.002
0	5	0.65	20	60	0.05%	0.002
5	0	0.65	20	60	0.49%	0.006
5	5	0.65	20	60	0.58%	0.006
10	10	0.65	20	60	1.18%	0.007
0	0	0.25	20	60	0.10%	0.003
5	5	0.25	20	60	0.87%	0.005
0	0	0.65	20	20	0.05%	0.002
5	5	0.65	20	20	0.63%	0.006
0	0	0.65	10	60	0.003%	0.0004
5	5	0.65	10	60	0.08%	0.002
0	0	0.65	40	60	0.23%	0.005
5	5	0.65	40	60	2.81%	0.012
0	0	0.65	20	40	0.03%	0.002
5	5	0.65	20	40	0.59%	0.006

Table 2*: Average percentage of matrix chains that wet the grafted layer as a function of graft and matrix lengths, grafting density and flexibility.*

As stated earlier, the reduced conformational entropy loss of the semi-flexible matrix chains is evident from the increase in average matrix end-end distance with decreasing flexibility (Table 1). However, the distribution of end-end distances of matrix upon wetting (Table 1 average and standard deviations in end-end distances for unwet and wet matrix chains) is not significantly different for flexible and semiflexible matrix chains (Table 1). This suggests that the reduced loss in conformational entropy of matrix chains with decreasing matrix flexibility is likely small. Conversely, at constant matrix flexibility, decreasing the grafted flexibility increases the brush height dramatically and results in significantly higher grafted layer volume, which increases the entropy of mixing of the grafted and matrix chains without altering significantly the conformational entropy loss of the matrix chains (Table 1 shows that matrix end-end distance remains the same). The likely increased gain in entropy of mixing of the graft and matrix chains,

quantified in Figure 10 and discussed in detail next, is driving the improved wetting behavior. While having both semiflexible graft and semiflexible matrix chains improves the wetting behavior the most over the other cases (Figure 9), the above data show that decreasing the graft flexibility, rather than matrix flexibility, has a larger impact on the wetting of the grafted layer by matrix chains.

To quantitatively assess how decreasing chain flexibility affects the mixing entropy of the grafted and matrix chains, we present, in Figure 10, the gain in mixing entropy versus decreasing flexibility (or increasing K) for graft and matrix polymers. In Figure 10, where the mixing entropy is calculated from the simulation trajectories by explicitly counting the number of matrix monomers that wet the grafted layer, we find that the total gain in mixing entropy of wetting the grafted layer by matrix chains, $T\Delta S_{mix}$, is much larger when the graft polymer flexibility is decreased than when the matrix polymer flexibility is decreased. Furthermore, as the flexibility of both graft and matrix polymers is decreased simultaneously, we see the largest increase in the gain in mixing entropy of wetting. This gain in mixing entropy is largest when both the grafts and matrix are at the minimum flexibility studied here (K_{graft}=10, K_{matrix}=10).

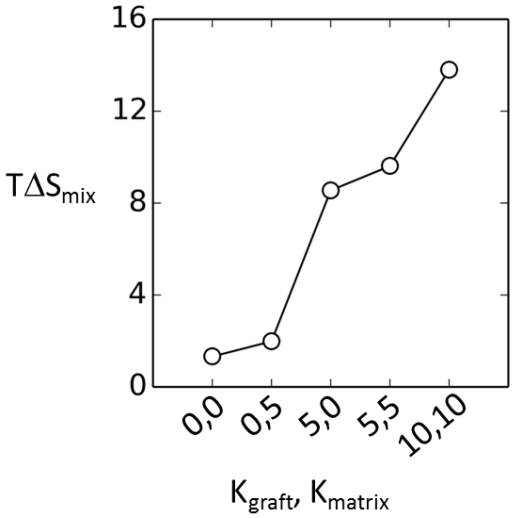

Figure 10: *Gain in mixing entropy, $T\Delta S_{mix}$ (in units of k_BT) as a function of graft and matrix flexibility.*

To summarize, with decreasing flexibility, increasing mixing entropy gains match well with the increasing of wetting of the grafted layer, while the changes in the end-end distances of the matrix chains upon wetting are minimal, therefore we can conclusively say that the mixing entropy of the grafted and matrix chains is a primary driving for wetting/dewetting in this system and that flexibility of the grafted and matrix chains directly tunes this driving force.

Having established that the wetting of polymer grafted particles in a polymer matrix is altered by decreasing flexibility of the graft and matrix polymers, we next investigate how decreasing polymer flexibility affects known trends of the effect of grafted density and matrix length on grafted layer wetting and nanocomposite morphology.

Effect of polymer flexibility on trends of grafting density on wetting/dewetting

For flexible graft and matrix polymers, where the matrix length is greater than graft length, as grafting density increases, wetting of the grafted layer decreases due to increased crowding in the grafted layer[23]. As the flexibility of graft and matrix polymer chains is reduced, we see that the effect of changing the grafting density on grafted layer wetting seems qualitatively unaltered, as seen in Figure 11. However, the percent change in the number of matrix monomers that have wet the grafted layer with increasing grafting density, normalized by the lower grafting density, shows a 70% drop for K=0 and a 33% drop for K=5. This suggests that the effect of increasing grafting density on wetting of the grafted layer is reduced with decreasing flexibility. We justify this trend as follows: For flexible grafted polymers at low grafting densities, the brush height is small because the grafted chains adopt mushroom conformations on the particle. As the grafting density increases, the grafted chains adopt extended conformations and the brush height increases. In contrast, for grafted polymers with reduced flexibility, at low grafting densities, the grafted chain conformations are extended to some degree, resulting in a larger brush height than the corresponding flexible grafted polymer, and therefore significantly improved wetting. As the grafting density increases, the change in brush height for grafted chains with reduced flexibility (Figure 11b) is lower than that for flexible grafted chains (Figure 11a). This is also confirmed by the change in average radius of gyration of grafted polymer chains with increasing grafting density being smaller for semiflexible polymers than flexible polymers (Table 3). In short, decreasing the flexibility reduces the effect of grafting density on the graft conformations, brush height, and wetting behavior.

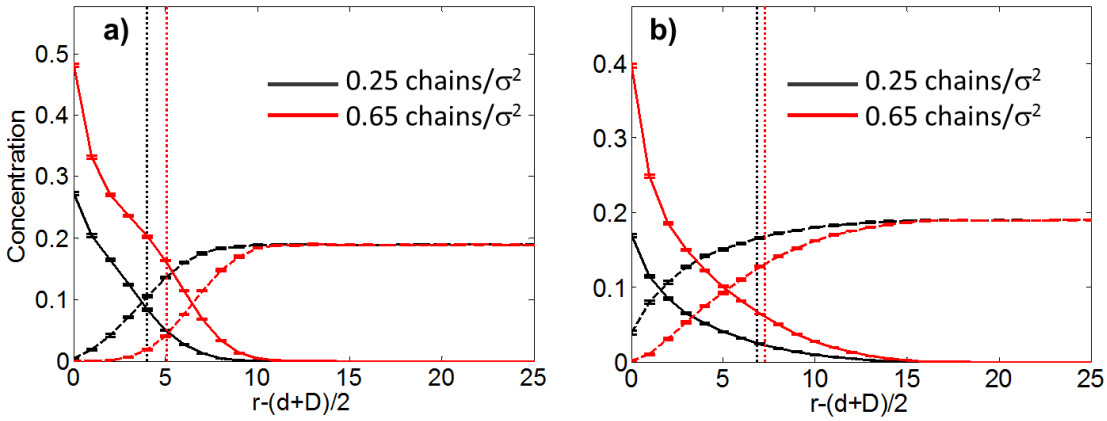

Figure 11: *Graft (solid) and matrix (dashed) monomer concentration profile for single polymer grafted particle with particle diameter 5nm, polymer grafting density=0.25 (black) and 0.65(red) chains/nm^2, and graft length=20 and matrix length =60 segments. The grafted layer "brush" heights are shown with dotted lines. The polymers in subplot a) have K_{graft} =0 and K_{matrix} =0, and in subplot b) have K_{graft} =5 and K_{matrix} =5.*

Table 3 Graft Radius of Gyration

K_{graft}	K_{matrix}	Grafting Density (chains/σ^2)	N_{graft}	N_{matrix}	$(Rg^2)^{1/2}$ (σ)
0	0	0.65	20	60	3.0
0	5	0.65	20	60	2.9
5	0	0.65	20	60	4.5
5	5	0.65	20	60	4.5
10	10	0.65	20	60	5.0
0	0	0.25	20	60	2.8
5	5	0.25	20	60	4.4
0	0	0.65	20	20	3.0
5	5	0.65	20	20	4.5
0	0	0.65	10	60	1.9
5	5	0.65	10	60	2.6
0	0	0.65	40	60	4.4
5	5	0.65	40	60	7.4
0	0	0.65	20	40	2.9
5	5	0.65	20	40	4.5

Table 3*: Table of graft radius of gyration for the measured parameters.*

Effect of polymer flexibility on trends of varying matrix polymer length on wetting/dewetting

In the case of flexible polymers, it is known that as the *matrix* polymer chain length increases at constant graft length, the wetting of the grafted layer by the matrix chains decreases. In Figure 12, despite the different shapes of the graft and matrix monomer concentration profiles with decreasing flexibility, we see that decreasing flexibility does not alter how the wetting of the grafted layer by the matrix chains changes with increasing matrix chain length, both visually as well as quantitatively (using data in Table 2). Our reasoning for this is as follow. In the flexible polymers case, the loss in conformational entropy of the matrix chain upon wetting the grafted layer is expected to increase slightly as the matrix polymer chain length increases (at constant graft length). Even though we know that as the flexibility decreases the matrix polymer conformational entropy decreases, both in the unwet and wet states, the trend of increasing loss in conformational entropy of the matrix chain upon wetting with increasing matrix length is likely the same as that in the completely flexible case.

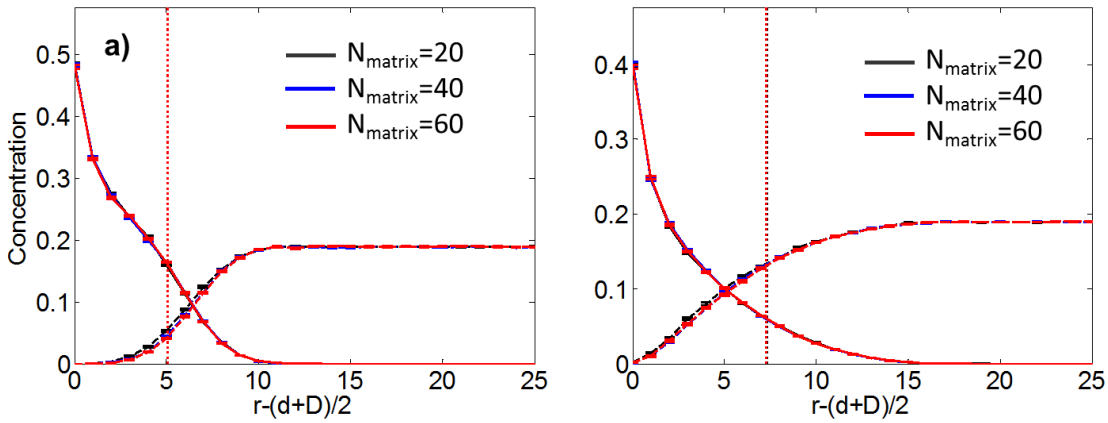

Figure 12: *Graft (solid) and matrix (dashed) monomer concentration profile for single polymer grafted particle with particle diameter 5nm, polymer grafting density= 0.65 chains/nm^2, and graft length=20 and matrix length =20 (black) and 60(red) segments. The grafted layer "brush" heights are shown with dotted lines. The polymers in subplot a) have K_{graft} =0 and K_{matrix} =0, and in subplot b) have K_{graft} =5 and K_{matrix} =5.*

Effect of polymer flexibility on trends of graft polymer length on wetting/dewetting

In the case of flexible polymers, it is known that as the *graft* polymer length increases, at constant matrix length, the wetting of the grafted layer by matrix chains increases. At short graft lengths, the grafted chains are extended because of the crowding around the particle surface, regardless of the flexibility of the polymer. As the graft length increases, the flexible polymer chains adopt coiled conformations at larger distances from the particle surface.[71] In contrast, graft polymers with reduced flexibility do not adopt coiled conformations and exhibit a larger brush height than corresponding flexible grafts. In Figure 13, the brush height increase with increasing graft length is much larger for semiflexible grafts than flexible grafts. Furthermore, due to smaller changes in the brush height between flexible grafts and grafts with decreased flexibility for short graft lengths, the short grafts do not experience as large an improvement in wetting due to the decrease in flexibility as the long graft lengths do. Using the data in Table 2, for semi-flexible polymers and N_{matrix}=60, going from graft length of 10 to 20, the wetting increases approximately 7 times and going from graft length of 10 to 40 the wetting increases about 35 times. In contrast for flexible polymers, going from graft length of 10 to 20, the wetting increases 10 times and going from 10 to 40 the wetting increases 77 times. This suggests that with decreasing flexibility of graft and matrix polymers, the effect of increased graft length on wetting of the grafted layer is reduced.

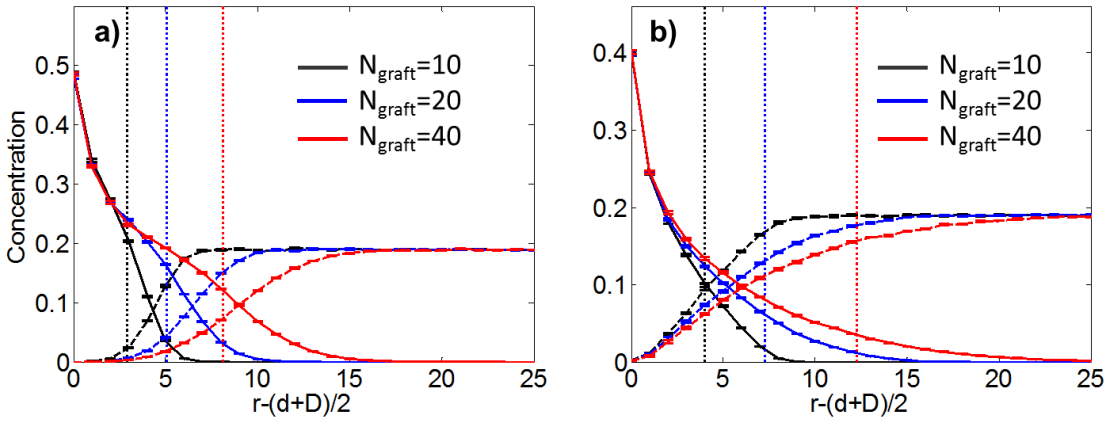

Figure 13: *Graft (solid) and matrix (dashed) monomer concentration profile for single polymer grafted particle with particle diameter 5nm, polymer grafting density= 0.65 chains/nm^2, and graft length=10 (black) and 20 (red) and matrix length =60 segments. The grafted layer "brush" heights are shown with dotted lines. The polymers in subplot a) have K_{graft} =0 and K_{matrix} =0, and in subplot b) have K_{graft} =5 and K_{matrix} =5.*

Effect of polymer flexibility on particle assembly/dispersion at higher filler fraction

Figure 14 shows that, in grafted particle systems at higher filler fractions, we continue to see the improved wetting with decreasing polymer flexibility that is seen at the single grafted particle limit. Since increasing wetting of the grafted layer has been connected to increased dispersion for flexible systems in past studies,[31-33] there could be improved dispersion of the grafted particles with decreasing flexibility of the polymers.

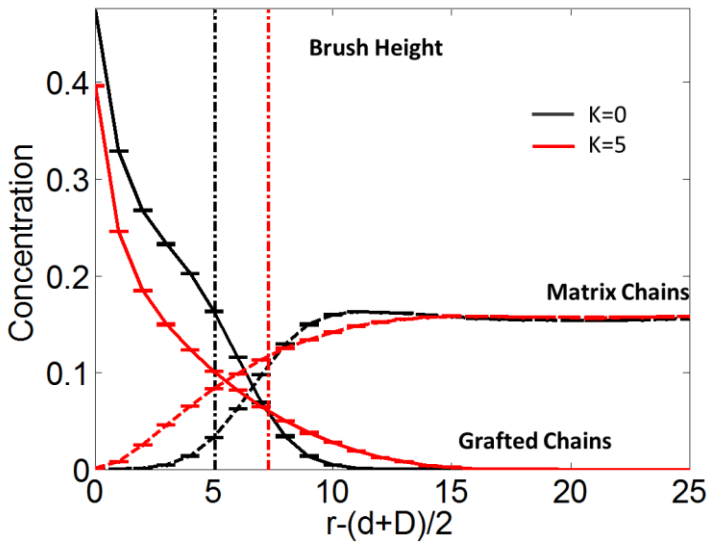

***Figure 14**: Graft (solid) and matrix (dashed) monomer concentration profile for 20 polymer grafted particles with particle diameter 5nm, polymer grafting density=0.65/nm^2, and graft length=20 and matrix length =100 segments. The grafted layer brush height, $\langle H_B^2 \rangle^{0.5}$, is shown in dotted lines. Decreasing flexibility is denoted by increasing values of three-body angle constant K_{graft} =0 and K_{matrix} =0 (black), K_{graft}=5 and K_{matrix}=5 (red).*

Figure 15 shows the particle-particle pair correlation function and therefore the degree of particle aggregation/dispersion in polymer nanocomposites with flexible and semiflexible polymers. In Figure 15, we remove the effect of the increased brush height with decreasing flexibility (see x-axis of the plot), in order to focus purely on the level of dispersion/aggregation of the grafted particles brought about by the changing flexibility of the polymers. When compared to the flexible graft and matrix polymer case, the particle-particle pair correlation for the semiflexible graft and matrix case shows a reduced correlation at the contact peak, with the contact peak shifting to larger distances. This confirms that reducing flexibility in graft and matrix polymers improves dispersion of the polymer grafted particles in a chemically identical polymer matrix, due to increased wetting of the grafted layer by matrix chains.

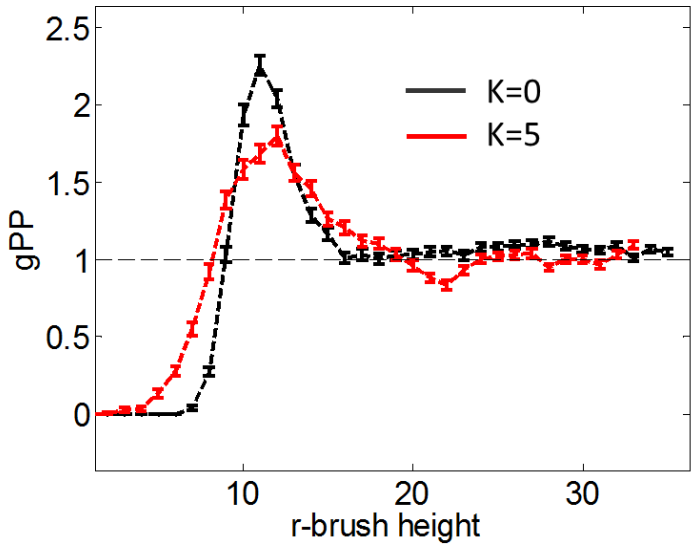

***Figure 15**: Particle-particle pair correlation function for 20 polymer grafted particles with particle diameter 5σ, polymer grafting density=0.65chains/σ^2, and graft length=20 and matrix length =100 segments plotted versus the interparticle distance minus the brush height. Decreasing flexibility is denoted by increasing values of K =0 (black) and 5(red).*

Conclusion

In summary, using molecular dynamics simulations we have shown that the wetting of polymer grafted particles by chemically identical matrix polymers is strongly dependent on the flexibility of the polymer chains. Decreasing flexibility of the grafted chains more significantly improves the wetting of the grafted layer than decreasing flexibility of the matrix chains. The gain in mixing entropy is significantly increased with decreasing graft polymer flexibility. While decreasing matrix flexibility reduces the loss in matrix conformational entropy upon wetting, we expect this reduction in matrix chain conformational entropy loss with decreasing matrix flexibility to be significantly smaller than the increase in mixing entropy gain with decreasing graft flexibility. Multi-particle or finite filler fraction simulations show that decreasing flexibility results in a shift of the contact peak in the particle-particle pair correlation function to higher

distances and reduction in the height of the contact peak, suggesting improved dispersion due to increasing wetting as predicted by the single particle simulations.

These effects of flexibility on wetting behavior suggest that in grafted nanoparticle filled nanocomposites with larger persistence length polymers (graft and matrix) one would see a larger window in the phase space where the particles would be dispersed. This could have implications in applications where high persistence length polymer nanocomposites are used.

IV: Summary

We have presented two computational simulation studies thus far that have broadened the design space for functionalized nanoparticles by providing an additional parameter that can affect the resulting assembly behavior. By changing the particle shape in Chapter 1, we demonstrated several unique assembly structures not seen with spherical particles. By changing the graft and matrix chain flexibility in Chapter 2, we presented new information about how a key polymer parameter can affect the assembly and dispersion of the grafted particles.

References

[1] G. Mattei, P. Mazzoldi and H. Bernas, "Metal nanoclusters for optical properties" Materials Science with Ion Beams, 2010, vol. 116, pp. 287–316.

[2] V. M. Shalaev, W. S. Cai, U. K. Chettiar, H. K. Yuan, A. K. Sarychev, V. P. Drachev and A. V. Kildishev, "Negative index of refraction in optical metamaterials" Opt. Lett., 2005, 30, 3356–3358.

[3] Balazs, A. C., Emrick, T., Russell, T.P., "Nanoparticle polymer composites: Where two small worlds meet" Science, 2006, 314, 1107-1110

[4] Bosman, A.W., Vestberg, R., Heumann, A., Frechet, J.M.J., Hawker, C.J., "A modular approach toward functionalized three-dimensional macromolecules: From synthetic concepts to practical applications" J. AM. CHEM. SOC. 2003, 125, 715-728

[5] Ohya, Y. et al, "Formation of 1D and 2D gold nanoparticle arrays by divalent DNA-gold nanoparticle conjugates", *Small*, 2012, 8, 2335-2340

[6] P. L. Biancaniello, A. J. Kim and J. C. Crocker, "Colloidal interactions and self-assembly using DNA hybridization" Phys. Rev. Lett., 2005, 94, 058302.

[7] D. B. Lukatsky, B. M. Mulder and D. Frenkel, "Designing ordered DNA-linked nanoparticle assemblies" J. Phys.: Condens. Matter, 2006, 18, S567–S580.

[8] Martin, T.B., Seifpour, A., Jayaraman, A, "Assembly of copolymer functionalized nanoparticles: a Monte Carlo simulation study" Soft Matter, 2011, 7, 5952-5964

[9] X. M. Jiang, B. Zhao, G. J. Zhong, N. X. Jin, J. M. Horton, L. Zhu, R. S. Hafner and T. P. Lodge, "Microphase Separation of high grafting density asymmetric mixed homopolymer brushes on silica particles" Macromolecules, 2010, 43, 8209–8217.

[10] J. U. Kim and M. W. Matsen, "Interaction between polymer-grafted particles" Macromolecules, 2008, 41, 4435–4443.

[11] Bera, R. K.; Raj, C. R, "A facile photochemical route for the synthesis of triangular Ag nanoplates and colorimetric sensing of H2O2" Journal of Photochemistry and Photobiology A: Chemistry 2013, (270) 1–6

[12] Jones, M. R.; Macfarlane, R. J.; Lee, B.; Zhang, J.; Young, K. L.; Senesi, A. J.; Mirkin, C. A. "DNA-nanoparticle superlattices formed from anisotropic building blocks" Nature Materials 2010, (9), 913-917

[13] Al-Ghamdi, H. S.; Mahmoud, W. E., "One pot synthesis of multi-plasmonic shapes of silver nanoparticles" Materials Letters 2013, (105), 62-64

[14] DuFort, C. C., Dragnea, B. "Bio-Enabled Synthesis of Metamaterials" Annu.Rev. Phys.Chem., 2010, 61, 323–344.

[15] Zhang, X.; Zhang, Z. L.; Glotzer, S. C., "Simulation study of cyclic-tethered nanocube self-assemblies: effect of tethered nanocube architectures " Nanotechnology 2007, (18), 1-6

[16] M. A. Horsch, Z. L. Zhang and S. C. Glotzer, “Self-assembly of polymer-tethered nanorods” Phys. Rev. Lett., 2005, 95, 056105.

[17] S. C. Glotzer, M. A. Horsch, C. R. Iacovella, Z. L. Zhang, E. R. Chan and X. Zhang, “Self-assembly of anisotropic tethered nanoparticle shape amphiphiles” Curr. Opin. Colloid Interface Sci., 2005, 10, 287–295.

[18] S. C. Glotzer and J. A. Anderson, “Nanoparticle assembly: Made to order” Nat. Mater., 2010, 9, 885–887.

[19] Kohlstedt, K. L.; Olvera de la Cruz, M.; Schatz, G. C., “Controlling orientational order in 1-D assemblies of multivalent triangular prisms” J. Phys. Chem. Lett. 2013, (4), 203-208

[20] Hall, L. M.; Jayaraman, A.; Schweizer, K. S. “Molecular theories of polymer nanocomposites” Current Opinion in Solid State & Materials Science 2010, 14, (2), 38-48.

[21] Jayaraman, A.; Nair, N. “Integrating PRISM theory and Monte Carlo simulation to study polymer-functionalised particles and polymer nanocomposites” Molecular Simulation 2012, 38, (8-9), 751-761.

[22] Jayaraman, A. “Polymer Grafted Nanoparticles: Effect of Chemical and Physical Heterogeneity in Polymer Grafts on Particle Assembly and Dispersion” Journal of Polymer Science Part B-Polymer Physics 2013, 51, (7), 524-534.

[23] Ganesan, V.; Jayaraman, A. “Theory and simulation studies of effective interactions, phase behavior and morphology in polymer nanocomposites” Soft Matter 2014, 10, (1), 13-38.

[24] Kumar, S. K.; Jouault, N.; Benicewicz, B.; Neely, T. “Nanocomposites with Polymer Grafted Nanoparticles” Macromolecules 2013, 46, (9), 3199-3214.

[25] Kumar, S. K.; Krishnamoorthi, R. “Nanocomposites: Structure, Phase Behavior, and Properties” Annual Review of Chemical and Biomolecular Engineering 2010, 1 37-58.

[26] P. F. Green, “The structure of chain end-grafted nanoparticle homopolymer nanocomposites” Soft Matter 2011, 7, 7914–7926.

[27] Goyal, S.; Escobedo, F. A. “Structure and transport properties of polymer grafted nanoparticles” Journal of Chemical Physics 2011, 135, (18), 184902.

[28] P. Akcora, H. Liu, S. K. Kumar, J. Moll, Y. Li, B. C. Benicewicz, L. S. Schadler, D. Acehan, A. Z. Panagiotopoulos, V. Pryamitsyn, V. Ganesan, J. Ilavsky, P. Thiyagarajan, R. H. Colby, J. F. Douglas, “Anisotropic self-assembly of spherical polymer-grafted nanoparticles” Nat. Mater. 2009, 8, U354–U121.

[29] Trombly, D. M.; Ganesan, V. “Curvature effects upon interactions of polymer-grafted nanoparticles in chemically identical polymer matrices” Journal of Chemical Physics 2010, 133, (15), 154904

[30] Nair, N.; Wentzel, N.; Jayaraman, A. “Effect of bidispersity in grafted chain length on grafted chain conformations and potential of mean force between polymer grafted nanoparticles in a homopolymer matrix” Journal of Chemical Physics 2011, 134, (19).

[31] T. B. Martin, P. M. Dodd, A. Jayaraman, “Polydispersity for Tuning the Potential of Mean Force between Polymer Grafted Nanoparticles in a Polymer Matrix” Phys. Rev. Lett. 2013, 110, 018301

[32] Martin, T. B.; Jayaraman, A. “Identifying the Ideal Characteristics of the Grafted Polymer Chain Length Distribution for Maximizing Dispersion of Polymer Grafted Nanoparticles in a Polymer Matrix” Macromolecules 2013, 46, (22), 9144-9150.

[33] Martin, T. B.; Jayaraman, A. “Polydisperse homopolymer grafts stabilize dispersions of nanoparticles in a chemically identical homopolymer matrix: an integrated theory and simulation study” Soft Matter 2013, 9, (29), 6876-6889.

[34] Rungta, A.; Natarajan, B.; Neely, T.; Dukes, D.; Schadler, L. S.; Benicewicz, B. C. “Grafting Bimodal Polymer Brushes on Nanoparticles Using Controlled Radical Polymerization” Macromolecules 2012, 45, (23), 9303-9311.

[35] A. Jayaraman and K. S. Schweizer, “Effective Interactions and Self-Assembly of Hybrid Polymer Grafted Nanoparticles in a Homopolymer Matrix” Macromolecules 42, 8423 (2009).

[36] Dijkstra, M.; Frenkel, D. “Simulation study of the isotropic-to-nematic transitions of semiflexible polymers” *Physical Review E* **1995,** 51, (6), 5891-5898.

[37] Dupre, D. B.; Yang, S. J. “Liquid-crystalline properties of solutions of persistent polymer-chains” *Journal of Chemical Physics* **1991,** 94, (11), 7466-7477.

[38] Fynewever, H.; Yethiraj, A. “Phase behavior of semiflexible tangent hard sphere chains” *Journal of Chemical Physics* **1998,** 108, (4), 1636-1644.

[39] Ivanov, V. A.; Stukan, M. R.; Vasilevskaya, V. V.; Paul, W.; Binder, K. “Structures of stiff macromolecules of finite chain length near the coil-globule transition: A Monte Carlo simulation” *Macromolecular Theory and Simulations* **2000,** 9, (8), 488-499.

[40] Jaffer, K. M.; Opps, S. B.; Sullivan, D. E.; Nickel, B. G.; Mederos, L. “The nematic-isotropic phase transition in semiflexible fused hard-sphere chain fluids” *Journal of Chemical Physics* **2001,** 114, (7), 3314-3324.

[41] Kindt, J. T.; Gelbart, W. M. “Chain self-assembly and phase transitions in semiflexible polymer systems” *Journal of Chemical Physics* **2001,** 114, (3), 1432-1439.

[42] Kong, M.; Dalal, I. S.; Li, G.; Larson, R. G. “Systematic Coarse-Graining of the Dynamics of Self-Attractive Semiflexible Polymers” *Macromolecules* **2014,** 47, (4), 1494-1502.

[43] Milchev, A. “Phase-transitions in polydisperse polymer melts” *Polymer* **1993,** 34, (2), 362-368.

[44] Pedersen, J. S.; Laso, M.; Schurtenberger, P. “Monte Carlo study of excluded volume effects in wormlike micelles and semiflexible polymers” *Physical Review E* **1996,** 54, (6), R5917-R5920.

[45] Schnurr, B.; Gittes, F.; MacKintosh, F. C. “Metastable intermediates in the condensation of semiflexible polymers” *Physical Review E* **2002,** 65, (6).

[46] Steinhauser, M. O. “Static and dynamic scaling of semiflexible polymer chains-a molecular dynamics simulation study of single chains and melts” *Mechanics of Time-Dependent Materials* **2008,** 12, (4), 291-312.

[47] Stukan, M. R.; Ivanov, V. A.; Grosberg, A. Y.; Paul, W.; Binder, K. “Chain length dependence of the state diagram of a single stiff-chain macromolecule: Theory and Monte Carlo simulation” *Journal of Chemical Physics* **2003,** 118, (7), 3392-3400.

[48] Wiggins, P. A.; Nelson, P. C. “Generalized theory of semiflexible polymers” *Physical Review E* **2006,** 73, (3).

[49] Wilhelm, J.; Frey, E. “Radial distribution function of semiflexible polymers” *Phys. Rev. Lett.* **1996,** 77, (12), 2581-2584.

[50] Yethiraj, A.; Fynewever, H. “Isotropic to nematic transition in semiflexible polymer melts” *Molecular Physics* **1998,** 93, (5), 693-701.

[51] Yethiraj, A.; Schweizer, K. S. “Integral-equation theory of polymer blends - numerical investigation of molecular closure approximations” *Journal of Chemical Physics* **1993,** 98, (11), 9080-9093.

[52] Ivanov, V. A.; Rodionova, A. S.; Martemyanova, J. A.; Stukan, M. R.; Mueller, M.; Paul, W.; Binder, K. "Conformational Properties of Semiflexible Chains at Nematic Ordering Transitions in Thin Films: A Monte Carlo Simulation" Macromolecules 2014, 47, (3), 1206-1220.

[53] Morse, D. C.; Fredrickson, G. H. "Semiflexible polymers near interfaces" Phys. Rev. Lett. 1994, 73, (24), 3235-3238.

[54] Muralidhar, A.; Tree, D. R.; Wang, Y.; Dorfman, K. D. "Interplay between chain stiffness and excluded volume of semiflexible polymers confined in nanochannels" Journal of Chemical Physics 2014, 140, (8).

[55] Sintes, T.; Sumithra, K.; Straube, E. "Adsorption of semiflexible polymers on flat, homogeneous surfaces" Macromolecules 2001, 34, (5), 1352-1357.

[56] Tallury, S. S.; Pasquinelli, M. A. "Molecular Dynamics Simulations of Polymers with Stiff Backbones Interacting with Single-Walled Carbon Nanotubes" Journal of Physical Chemistry B 2010, 114, (29), 9349-9355.

[57] Ganesan, V.; Khounlavong, L.; Pryamitsyn, V. "Equilibrium characteristics of semiflexible polymer solutions near probe particles" Physical Review E 2008, 78, (5).

[58] Padmanabhan, V., Frischknecht, A.L., Mackay, M.E., "Effect of Chain Stiffness on Nanoparticle Segregation in Polymer/Nanoparticle Blends Near a substrate" Macromol. Theory Simul. 2012, 21, 98–105

[59] Xu, M.; Zhao, Q.; Zhang, C.; Du, Z.; Mi, J. "Integral Equation Prediction of Surface-Induced Layering Transition of Polymer Nanocomposites" Journal of Physical Chemistry C 2013, 117, (38), 19409-19418.

[60] Zhang, D.; Jiang, Y.; Wen, X.; Zhang, L. "Phase separation and crystallization of binary nanoparticles induced by polymer brushes" Soft Matter 2013, 9, (6), 1789-1797.

[61] Schnurr, B.; MacKintosh, F. C.; Williams, D. R. M. "Dynamical intermediates in the collapse of semiflexible polymers in poor solvents" Europhysics Letters 2000, 51, (3), 279-285.

[62] HOOMD-blue web page: http://codeblue.umich.edu/hoomd-blue

[63] J. A. Anderson, C. D. Lorenz, and A. Travesset. General purpose molecular dynamics simulations fully implemented on graphics processing units Journal of Computational Physics 227(10): 5342-5359, May 2008.

[64] T. D. Nguyen, C. L. Phillips, J. A. Anderson, and S. C. Glotzer. Rigid body constraints realized in massively-parallel molecular dynamics on graphics processing units Computer Physics Communications 182(11): 2313-2307, June 2011.

[65] Ceperley, D.; Kalos, M. H.; Lebowitz, J. L. "Computer Simulation of the Dynamics of a Single Polymer Chain" Phys. Rev. Lett. 1978, 41, (5), 313-316.

[66] Lennard-Jones, J. E. "On the determination of molecular fields" Proc. R. Soc. Lond. A 1924, 106 (738), 463–477

[67] Weeks, J. D.; Chandler, D.; Andersen, H. C. J. "Role of repulsive forces in determining equilibrium structure of simple liquids" Chem. Phys. 1971, (54), 5237

[68] A. Grossfield, WHAM: the weighted histogram analysis method, version 2.0.4, http://membrane.urmc.rochester.edu/content/wham.

[69] Winkler, R. G.; Reineker, P.; Harnau, L. “Models and equilibrium properties of stiff molecular chains” The Journal of Chemical Physics 1994, 101, (9), 8119-8129.

[70] Hansen, J.-P.; McDonald, I. R., Theory of Simple Liquids 3rd ed.; 2006.

[71] Daoud, M.; Cotton, J. P. “Star shaped polymers - a model for the conformation and its concentration-dependence” Journal De Physique 1982, 43, (3), 531-538.

[72] Humphrey, W.; Dalke, A.; Schulten, K. VMD: Visual Molecular Dynamics. J. Mol. Graphics Modell. 1996, 14, 33−38a

Appendix

Snapshots created using VMD.[72]

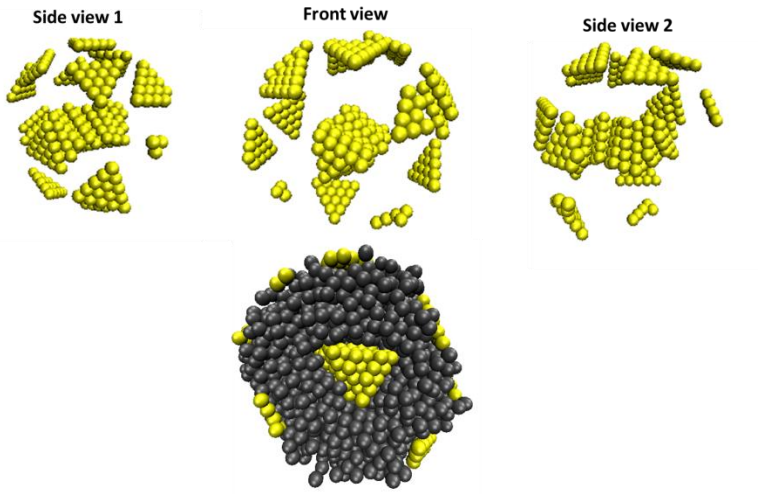

Figure A.1: *Simulation snapshot conveying the shell and stack structure from different views. Interaction set:* $\varepsilon_{PP}=0$ *and* $\varepsilon_{MM}=1$.

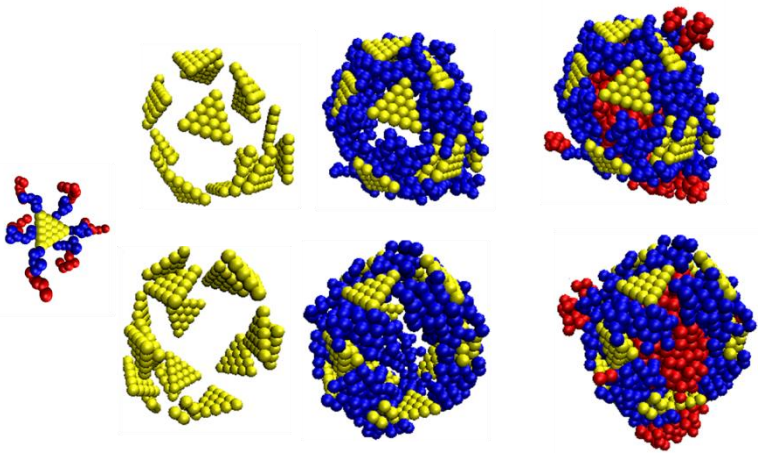

Figure A.2: *Simulation snapshot conveying the "the particles align along their edges and form a spherical shell-like structure, where the exterior of the shell is the particles followed by a shell of the inner A monomers followed by a core of the outer B monomers". Interaction set:* $\varepsilon_{PP}=0$ *and* $\varepsilon_{AA}=\varepsilon_{BB}=1$.

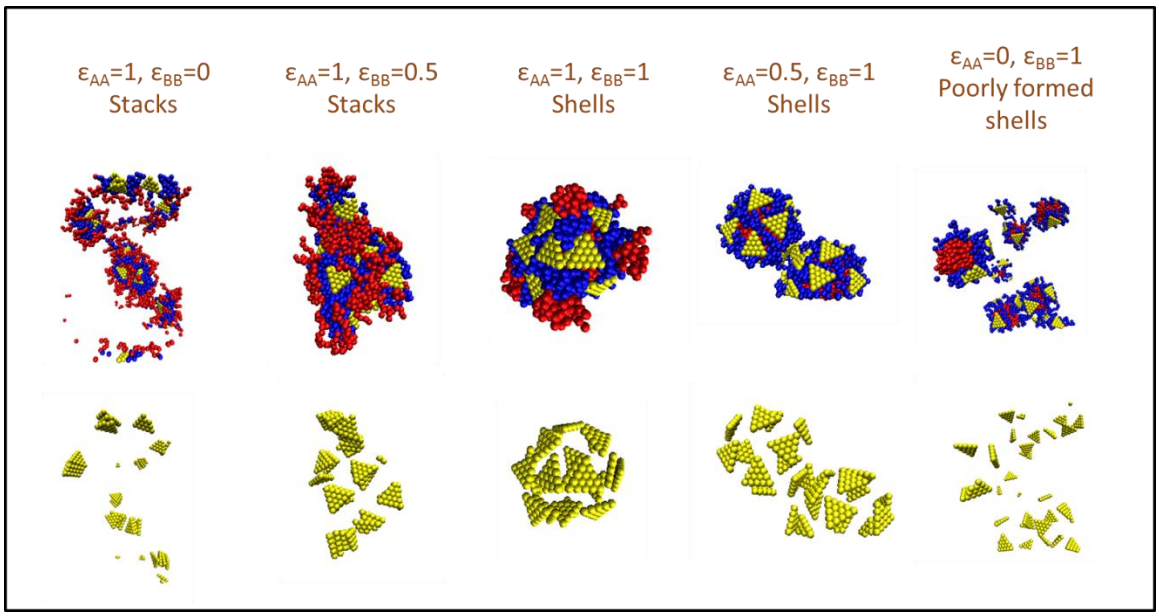

Figure A.3: *Representative simulation snapshots of copolymer functionalized nanoparticles with no particle-particle attraction. AA and BB attraction are varied from left to right.*

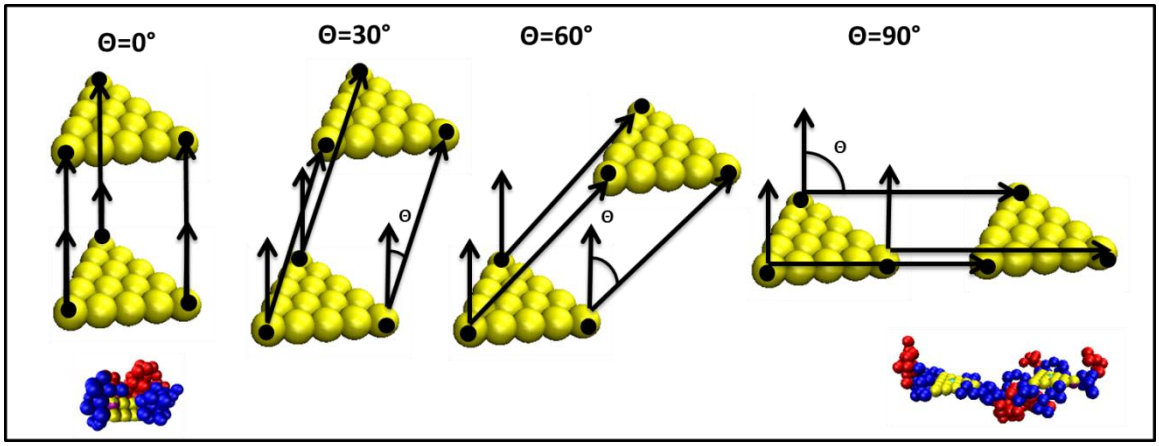

Figure A.4: *Schematic describing the biasing potential used to capture the orientation aspect of the PMF and to differentiate between shell and stack formation. At 0° angle, the bias is favoring the stacked orientation. At 30°-60° angles, the bias is favoring some of the orientations present in the shell structure. At the 90° angle, the bias is favoring the edge-on configuration.*

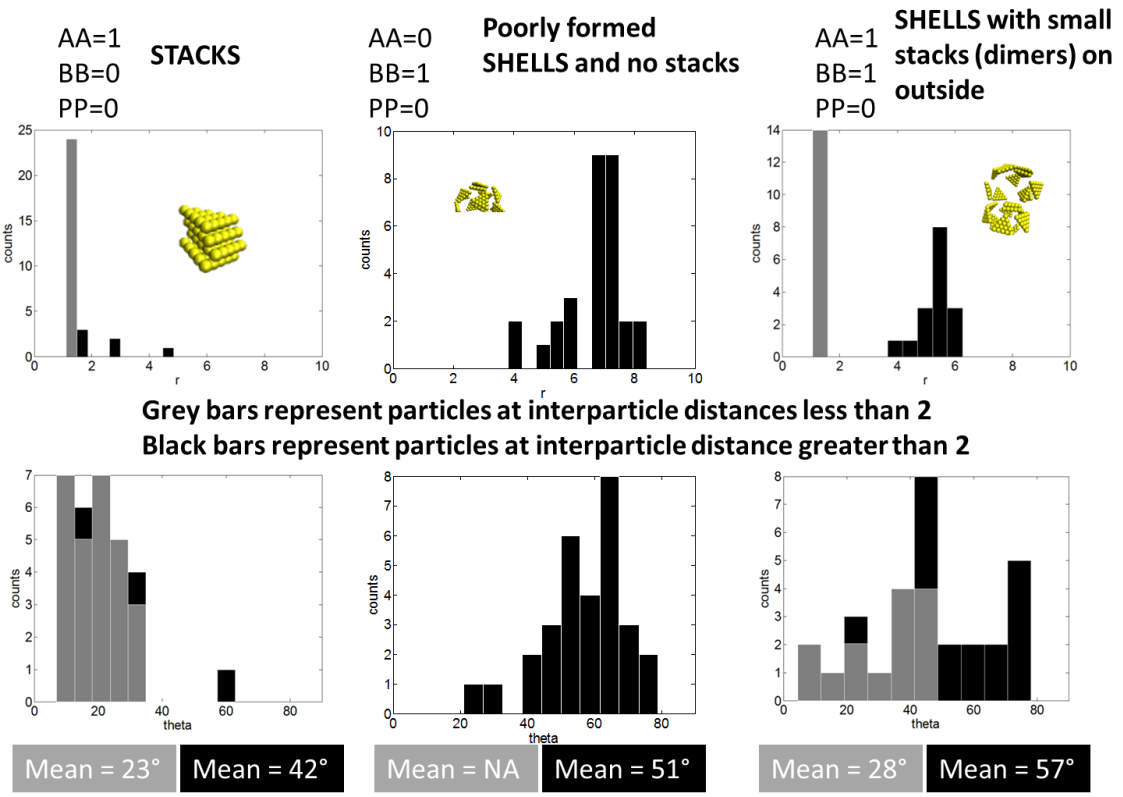

Figure A.5: *Nearest neighbor interparticle distance and angle histograms based on data from simulations with 30 particles. The top row depicts the interparticle distance histograms and the bottom row depicts the interparticle angle histograms. The left column depicts the a stack forming scenario (interaction set: $\varepsilon_{AA}=1$, $\varepsilon_{BB}=0$, $\varepsilon_{PP}=0$), the middle column depicts a poorly forming shell scenario (interaction set: $\varepsilon_{AA}=0$, $\varepsilon_{BB}=1$, $\varepsilon_{PP}=0$), and the right column depicts a strongly forming shell scenario that also forms a large number of stacks on the outside of the shell (interaction set: $\varepsilon_{AA}=1$, $\varepsilon_{BB}=1$, $\varepsilon_{PP}=0$). For clarity, the interparticle angles that occur at distances < 2 (stacking distances) are colored grey, interparticle angles that occur at distances > 2 (shell forming distances) are colored black.*

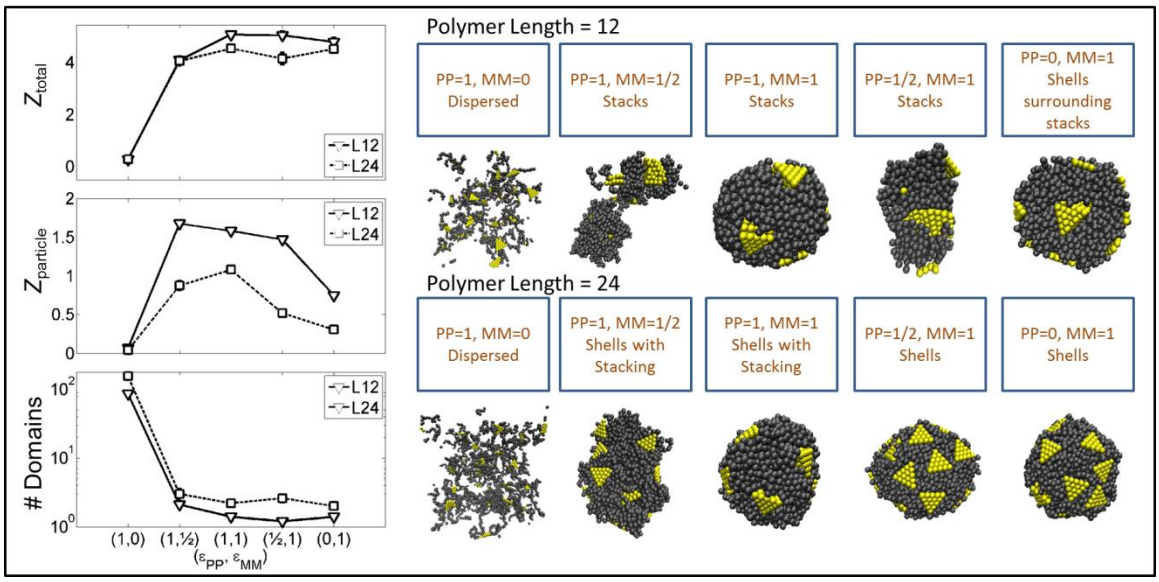

Figure A.6: *Shows the effect of changing homopolymer strand length. The plots on the left show the strand length 12 (solid triangles) and strand length 24 (dashed squares) versus changing particle-particle and monomer-monomer attractions. The representative simulation snapshots on the right correspond to each of the interaction sets plotted with the top row depicting strand length 12 and the bottom row depicting strand length 24.*

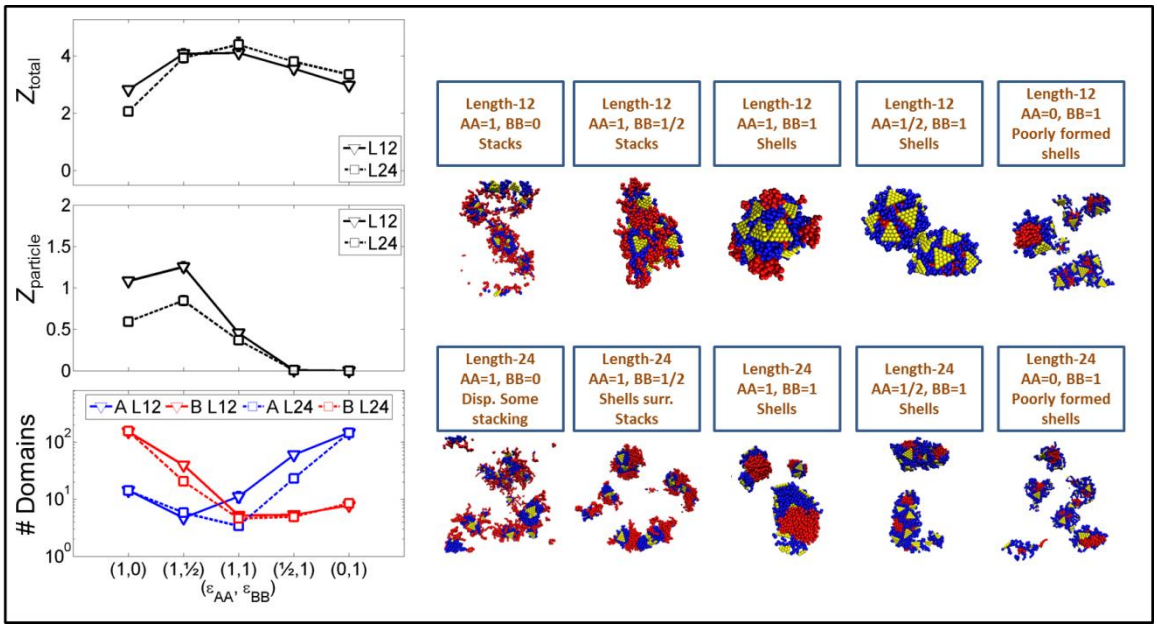

Figure A.7: *Shows the effect of changing copolymer strand length when particle-particle attraction is zero. The plots on the left show the strand length 12 (solid triangles) and strand length 24 (dashed squares) versus changing particle-particle and monomer-monomer attractions. The bottom left plot shows the number of both A (blue) and B (red) domains. The*

representative simulation snapshots on the right correspond to each of the interaction sets plotted with the top row depicting strand length 12 and the bottom row depicting strand length 24.

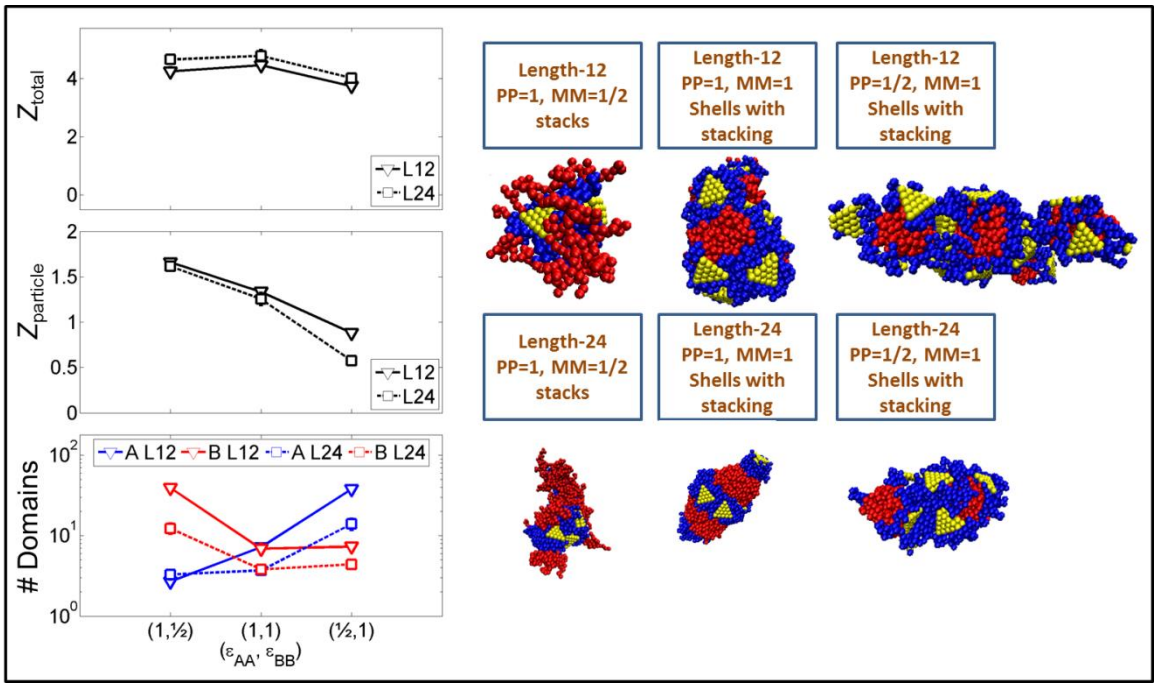

Figure A.8: *Shows the effect of changing copolymer strand length when $\varepsilon_{PP}=1$. The plots on the left show the strand length 12 (solid triangles) and strand length 24 (dashed squares) versus changing particle-particle and monomer-monomer attractions. The bottom left plot shows the number of both A (blue) and B (red) domains. The representative simulation snapshots on the right correspond to each of the interaction sets plotted with the top row depicting strand length 12 and the bottom row depicting strand length 24.*

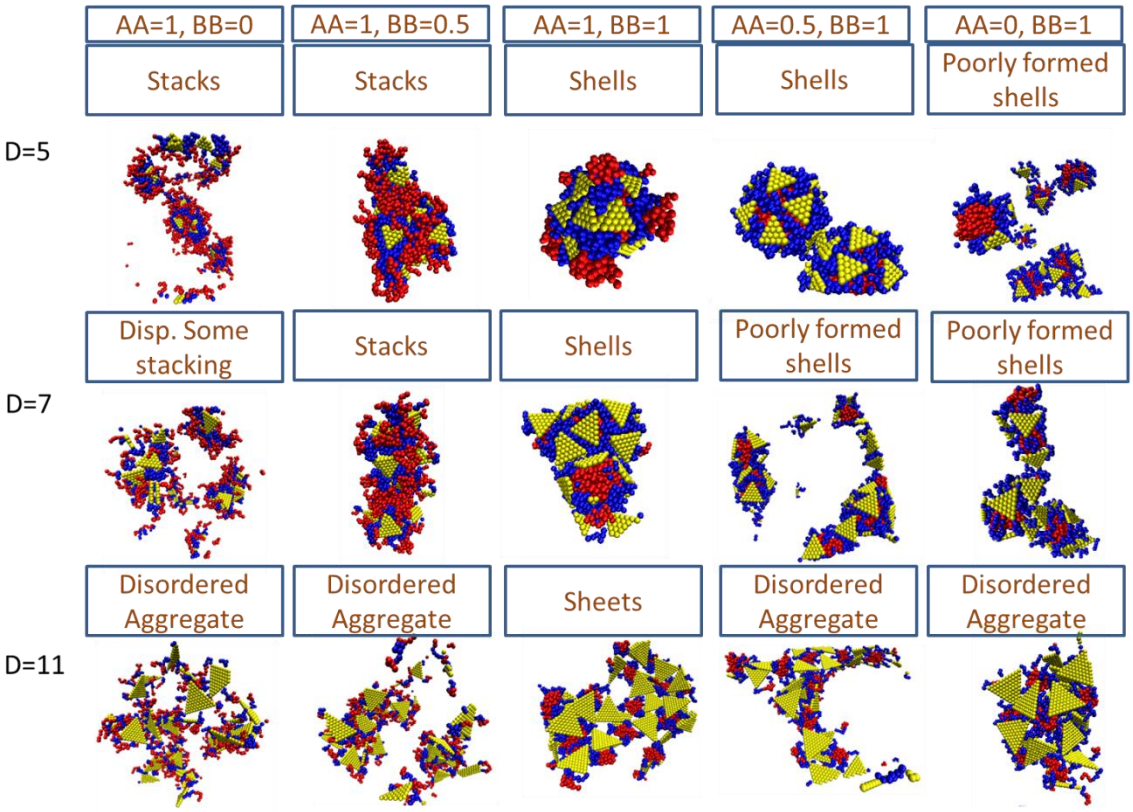

Figure A.9: *Shows representative simulation snapshots as particle size is changed. AA and BB attraction are varied from left to right. The top row depicts the snapshots for particle size 5, the middle row depicts snapshots for particle size 7, and the bottom row depicts snapshots for particle size 11.*